Materials Today Bio 30 (2025) 101398

Contents lists available at ScienceDirect

Materials Today Bio

journal homepage: www.journals.elsevier.com/materials-today-bio

Porcine pericardial decellularized matrix bilayer patch containing adipose stem cell-derived exosomes for the treatment of diabetic wounds

Wei Liang [a,1], Huiting Wu [a,1], Lindan Tan [b], Xiaoyu Meng [a], Wanwen Dang [a], Meng Han [a], Yonghuan Zhen [a], Haifeng Chen [b,***], Hongsen Bi [a,**], Yang An [a,*]

[a] Department of Plastic Surgery, Peking University Third Hospital, 49 North Garden Road, Haidian District, Beijing, 100191, China
[b] Department of Biomedical Engineering, College of Future Technology, Peking University, 5 Yiheyuan Road, Haidian District, Beijing, 100871, China

ARTICLE INFO

Keywords:
Decellularized porcine pericardium
Adipose-derived stem cell exosomes
Bilayer patche
Diabetic wounds

ABSTRACT

Chronic hard-to-heal wounds pose a significant threat to patients' health and quality of life, and their clinical management remains a challenge. Adipose-derived stem cell exosomes (ADSC-exos) have shown promising results in promoting diabetic wound healing. However, effectively enhancing the retention of exosomes in wounds for treatment remains a key issue that needs to be addressed. There is a pressing need to develop new materials or methods to improve the bioavailability of exosomes. Porcine pericardium, an extracellular matrix-rich tissue, is easily obtainable and widely available. Decellularized porcine pericardium removes cellular components while retaining an extracellular matrix that supports cellular growth, making it an ideal raw material for preparing wound dressings. In this study, we developed porcine pericardial decellularized matrix bilayer patches loaded with ADSC-exos, which were transplanted into diabetic mouse skin wounds. Histological and immunohistochemical analyses revealed that these bilayer matrix patches accelerate wound healing by promoting granulation tissue formation, re-epithelialization, stimulating vascularization, and enhancing collagen production. In terms of the underlying biological mechanism, we found that decellularized extracellular matrix bilayer patches loaded with ADSC-exos enhanced the proliferation and migration of human dermal fibroblasts (HDFs) and HaCaT cells in vitro, and promoted tube formation in human umbilical vein endothelial cells (HUVECs). This research demonstrated that the porcine pericardial decellularized matrix is well-suited for exosome delivery and that these bilayer patches hold great potential in promoting diabetic wound healing, providing evidence to support the future clinical application of ADSC-exos.

1. Introduction

Chronic hard-to-heal wounds threaten patients' health and quality of life, and their clinical management remains challenging [1]. Among them, due to diabetic wounds in the inflammatory stage of stagnation or infection, the wound will evolve into a chronic diabetic hard-to-heal wounds [2], seriously affecting the patient's daily life, and in severe cases even lead to amputation and death. Currently, wound dressings, debridement surgery, laser therapy, negative pressure wound therapy [3], and hyperbaric oxygen are used for symptomatic management of wounds in clinical practice [4], but there are many drawbacks, such as limited supply, high manufacturing costs, severe inflammatory reactions, various disease risks, and the quality of wound healing is not high enough [5], and the ideal wound dressing has not yet been developed [6].

As an emerging therapeutic approach in regenerative medicine, stem cell-based tissue regeneration research has received widespread attention. The goal of stem cell therapy is to restore or replace dysfunctional tissues and organs through stem cell pluripotency, self-renewal, and regenerative cytokine secretion [7]. Compared with the direct use of stem cells, the use of exosomes for wound treatment has the advantages of low immunogenicity, easy storage and quantification [8]. However, how to optimize its extraction protocol and use effect has been a difficult problem in the study of exosomes [9], so there is a need to develop new

* Corresponding author.
** Corresponding author.
*** Corresponding author.
E-mail addresses: haifeng.chen@pku.edu.cn (H. Chen), bihongsen@bjmu.edu.cn (H. Bi), anyangdoctor@163.com (Y. An).
[1] These authors contributed equally to this work.

https://doi.org/10.1016/j.mtbio.2024.101398
Received 9 August 2024; Received in revised form 1 November 2024; Accepted 9 December 2024
Available online 10 December 2024

materials or methods to improve the yield and bioavailability of exosomes to maximize their therapeutic effects. Adipose stem cell-derived exosomes (ADSC-exos) contain a variety of proteins and genetic material associated with tissue regeneration and wound healing [10]. Several studies have shown that ADSC-exos can accelerate cutaneous wound repair by participating in inflammation [11], angiogenesis [12,13], cell proliferation and extracellular matrix remodeling [14], as well as alleviating oxidative stress in the wound microenvironment [15]. In our previous study, we found that ADSC-exos can promote wound healing by regulating apoptosis and autophagy [16].

Decellularization is an emerging biomaterial preparation method in tissue engineering [17], which involves the removal of cellular components from biological tissues or organs to obtain a protein matrix for cell growth [18], which is ideal raw material for the preparation of wound dressings [19]. In many current studies on tissue regeneration, decellularized matrices of cardiac origin are attractive because they retain key molecules for wound healing, such as collagen, elastin, fibronectin and pro-angiogenic factors (ANG-1, ANG-3, CCN1, FGF-1, FGF-2, leptin, MMP-9, NOV, SDF-1 and VEGF -β) [20], which not only accelerates wound re-epithelialization to accelerate wound closure [21], but also improves healing quality by increasing collagen deposition and maturation. Porcine pericardium is an extracellular matrix dense tissue that is easily accessible and widely available [22,23]. Studies have shown that one of the major advantages of pericardium in the development of decellularized biomaterials is the high content of type I collagen, which is about 47 % [24]. In addition, the pericardium portion is sparsely populated with cells, a feature that allows for easy removal of biologic factors, such as DNA, from the tissue [25].

In this study, we prepared a porcine pericardial decellularized matrix, extracted adipose-derived stem cell exosomes by ultracentrifugation, and then combined collagen containing adipose-derived stem cell exosomes to form a bilayered patch, which exhibited good physical properties and biocompatibility. In skin cells, the patch could slowly release exosomes and promote cell proliferation, migration and tube formation. Next, we evaluated the therapeutic effect of the bilayer patch on wounds in diabetic mice. Overall, we provide a promising strategy for the application of exosomes in wound healing, and our patch can effectively promote angiogenesis, collagen deposition, re-epithelialization, cell proliferation and migration, and ultimately accelerate wound healing.

2. Materials and methods

2.1. Clinical specimen and animal ethics

6-8-week-old C57BL/6J male mice were provided by the Laboratory Animal Center of Peking University Third Hospital. Human subcutaneous fat aspirates were obtained from healthy females undergoing liposuction at the Third Hospital of Peking University after written informed consent was obtained, and all protocols were approved by the Ethics Committee of the Third Hospital of Peking University (Ethical approval number: M2022400). All animal experiments were approved by the Institutional Animal Care and Use Committee of the Third Hospital of Peking University and were performed according to the guidelines of the National Health Medical Research Council (Ethical approval number: A2022057).

2.2. Extraction and characterization of adipose stem cells and their exosomes

Fat aspirates obtained during liposuction were digested with 1 mg/mL of type I collagenase (Cellvis, 200110-50, USA) for 30 min at 37 °C in a shaking incubator. After digestion, the sample was filtered through a 200-mesh cell filter, and the resulting adipocyte suspension was centrifuged at 800 g for 5 min. The cell pellet at the bottom was then resuspended in PBS. After an additional centrifugation for 5 min, the cell pellet was resuspended in culture medium (DMEM/F12; Hyclone) supplemented with 10 % fetal bovine serum (FBS, C04001-050X10, Lablead, China) and 1 % penicillin-streptomycin (Hyclone). The cells were incubated at 37 °C with 5 % CO2. Upon reaching 80 % confluence, the adipose-derived stem cells (ADSCs) were passaged, and cells from passages 3 to 5 were used in this study.

The extracted stem cells were tested for pluripotency via flow cytometry and their ability to undergo tri-lineage differentiation. Adipose stem cells from the 3rd generation were used, and after digestion, the cells were resuspended in an appropriate amount of PBS (FG701-01, Transgen Biotech, Beijing, China). The cells were divided into five 1.5 mL EP tubes at a concentration of 1×10^6 cells per tube. The tubes were centrifuged at 1000 g for 3 min, and the supernatant was discarded. The cell pellets were incubated for 30 min at 4 °C, protected from light, in 100 μL of PBS. Next, 100 μL of PBS containing CD29, CD44, CD73, CD34, CD14, and CD45 antibodies was added to each tube. The samples were thoroughly mixed and incubated for 30 min at 4 °C in the dark. After incubation, the cells were centrifuged at 1000 g for 3 min, the supernatant was discarded, and the cells were washed twice with PBS. After a final centrifugation at 1000*g* for 3 min, the supernatant was removed. The cells were resuspended in 200 μL of PBS and analyzed using a flow cytometer (CytoFLEX S, Beckman). For the identification of adipogenic, osteogenic, and chondrogenic differentiation, 70–80 % confluent 3rd-generation adipose stem cells were seeded in 6-well plates. The cells were induced using lineage-specific induction media, stained for 10 min, and subsequently observed and photographed under a microscope.

Isolationand characterization of ADSC-exos: ADSCs were cultured in serum-free medium for 48 h to collect the cell supernatant. The supernatant was centrifuged at 1000 g for 10 min to remove dead cells. The remaining supernatant was then centrifuged at 6000 g for 6 min to eliminate cellular debris, followed by centrifugation at 12,000 g for 30 min to remove macromolecules. Finally, the sample was centrifuged at 100,000 g for 120 min. Exosomes were pelleted at the bottom of the ultracentrifuge tubes, and the supernatant was carefully aspirated. The exosome pellet was resuspended in 300 μL of PBS. The suspension was aliquoted into small centrifuge tubes and stored at −80 °C for later use. Before use, the exosomes were filtered through a 200 nm microporous membrane. The size of the purified exosomes was determined using a nanoparticle tracking analyzer (NS300, Malvern). The presence of CD63, CD81, and TSG101 proteins in the exosomes was confirmed by Western blot analysis. ADSC-exos were labeled with PKH26 Red Fluorescent Cell Linker Kit, according to the manufacturer's instructions (D0030, Beijing Solarbio Science & Technology Co., Ltd. China). The protein concentration of the exosomes was quantified using the Bicinchoninic Acid (BCA) Assay Kit (Beyotime, China). The ultrastructure of the extracellular vesicles was observed using transmission electron microscopy (TEM) with a Libra 120 instrument (Zeiss).

2.3. Cell proliferation, migration and tube formation experiments

Human keratinocytes (HaCaT), human umbilical vein endothelial cells (HUVECs), and human dermal fibroblasts (HDFs) were obtained from the Peking Union Medical College Cell Bank. All cell types were cultured in DMEM supplemented with 5 % fetal bovine serum (FBS, Shanghai Lian Shuo Biotechnology Co., Ltd.) and 1 % penicillin-streptomycin (Hyclone) at 37 °C in a 5 % CO_2 atmosphere.

For the cell proliferation assay, HaCaT and HDF cells were seeded at a density of 5×10^3 cells per well in 96-well culture plates, with 100 μL of the culture medium added to each well. The cells were stimulated with 0, 10, 30, or 50 μg/mL of ADSC-exosomes (ADSC-exos) for 1, 3, or 5 days, respectively. Cell proliferation activity was measured using the Cell Counting Kit-8 (CCK-8, AKCE001-1, Beijing Boxbio Science & Technology Co.,Ltd., China), and absorbance at 450 nm was recorded using a microplate reader.

For the Transwell experiments, cells were seeded at a density of 2×10^5/mL. A total of 600 μL of complete medium containing 0, 10, 30, or

50 μg/mL of exosomes was added to the lower chamber of a 24-well plate (AXYPCR24B, Corning, China). The Transwell insert (KTA5010, Abbkine, Wuhan,China) was carefully placed into the 24-well plate using tweezers, and 200 μL of the cell suspension was added to the upper chamber. The plate was then incubated for 48 h. After incubation, cells in the upper chamber were carefully removed by blotting them with tweezers.

To assess migration, the chambers were carefully removed, and the medium from the upper chamber was aspirated. The cells in the Matrigel and upper chamber were gently wiped away with a cotton swab. The chambers were then transferred to a new 24-well plate containing 600 μL of 4 % paraformaldehyde for fixation for 20–30 min. After fixation, the chambers were moved to wells containing approximately 800 μL of 0.2 % crystal violet solution for staining, which was pre-added to the wells. The chambers were stained for 30 min. Excess crystal violet was removed, and the upper side of the chambers was gently wiped with a cotton swab to eliminate non-specifically bound dye, facilitating cell counting in subsequent microscopic examinations.

Tube formation was assessed using the Matrigel method. Briefly, 50 μL of Matrigel matrix (BD Biosciences, San Jose, CA, USA) was added to each well of a 96-well plate and incubated at 37 °C to allow the gel to form. After 24 h of serum starvation, cells were seeded into the 96-well plate at a density of 5000 cells per well, and 100 μL of medium was added to each well. The cells were then stimulated with 0, 10, 30, and 50 μg/mL of ADSC-exosomes (ADSC-exos) for 24 h, and tube formation was observed under a microscope. The number of nodes, junctions, and meshes formed by the tubes in each field was quantified using ImageJ software.

2.4. Preparation of exosome-containing collagen-bound porcine pericardial decellularized extracellular matrix (dECM) bilayer patches

The lower layer of the composite patches was prepared using the decellularized extracellular matrix (dECM) from porcine pericardium as follows: The pericardium was carefully removed from the surface of fresh porcine hearts and soaked in Neosporin broad-spectrum disinfectant for 15 h. After soaking, the pericardium was treated with 3.0 % (by mass) acetone for 24 h to remove fat and fat-soluble impurities. It was then decellularized using 0.1 % (by mass) Triton X-100 (Cat No.1271889, Leyan, Shanghai, China) and pepsin under ultrasound at 30 kHz for 48 h to remove cells and cellular debris from the tissue. The decellularized pericardium was then treated with an amide active reagent at pH 7 for 48 h, followed by guanidine hydrochloride (8 mol/L) for 24 h to disrupt hydrogen bonds in collagen molecules and further remove fat and fat-soluble impurities. Collagen in the pericardium was crosslinked using polyethylene glycol (0.5 % by mass) at pH 7 for 48 h. The collagen-treated pericardium was freeze-dried at 10 Pa for 72 h. After drying, the decellularized pericardium matrix was sterilized using γ-radiation at a dose of 30 kGy.

The upper layer of the patches was made using rat tail type I collagen, either encapsulating or not encapsulating 50 μg of adipose stem cell exosomes. The following items were placed on ice: collagen I, sterile 10 × PBS, sterile distilled water, and sterile 1 M NaOH. Following the reagent instruction manual, NaOH and 10 × PBS were added to the collagen I to adjust the pH to 7. The collagen mixture was then applied to the lower decellularized pericardial membrane and allowed to solidify at room temperature for 30 min.

2.5. DNA content testing and H&E staining

The DNA content of the porcine pericardium before and after decellularization was measured using the Tissue DNA Kit (AA0901-A, Shandong Sparkjade Biotechnology Co., Ltd., China). Hematoxylin and eosin (H&E) staining was performed to verify the complete removal of cells from the decellularized pericardium.

2.6. Scanning electron microscope (SEM)

The microstructure of the decellularized pericardium and the prepared bilayer patches was observed using scanning electron microscopy (SEM, EVO 10, Zeiss). Additionally, exosomes were loaded onto circular bilayer matrix patches with a diameter of 1 cm, and the presence of exosome particles on the patches was subsequently detected by SEM.

2.7. Tensile modulus testing

The prepared bilayer matrix patches, which incorporated decellularized pericardium, were trimmed into rectangular shapes measuring 10 mm in length and 5 mm in width. The tensile modulus of the patches was evaluated using a biomechanical testing machine (MX 0580, Moshin). An initial force of approximately 0.1 N was applied to each sample, with a tensile speed of 2 mm/min. The resulting loads and displacements were recorded and plotted as stress-strain curves. Each set of samples consisted of six parallel groups to ensure reproducibility of the experiments.

2.8. Swelling ratio and degradation rates

For the swelling ratio assay, 15 mg of each bilayer matrix patch and decellularized pericardium were weighed and incubated in PBS at 37 °C for 4 h. Measurements were taken at time intervals of 0, 3, 9, 12, 15, 18, 24, and 27 h to assess the water absorption capacity of the patches. For the degradation rate assay, the patches were incubated in a collagenase solution (50 mg/mL collagenase I in 1 × PBS, pH 7.4) at 37 °C for 0, 2, 4, 6, 12, and 24 h, and in vitro degradation was observed. The patches were removed at each time point, dried, and weighed.

2.9. In vitro release of exosomes

The micro BCA kit (BioWorks, C503061-1250, China) was used to determine the encapsulation rate and release of exosomes in the bilayer patches, with bilayer patches without exosomes serving as the control. The protein concentrations for the standard curve were prepared according to the kit instructions. The average A562 value for each tube in the standard group was plotted on the vertical axis, and the corresponding protein concentration on the horizontal axis, to create the standard curve, either on graph paper or using Microsoft Excel. Based on the average A562 values from two dilutions of the same sample, the protein concentration of the diluted sample was calculated using the standard curve. The final protein concentration of the original sample was then determined by factoring in the appropriate dilution factor.

2.10. Cell growth and adhesion

Confocal microscopy was used to observe the growth of cells on the bilayer patches. Human skin fibroblasts, keratinocytes, and human umbilical vein endothelial cells (HUVECs) were cultured in serum-free medium for 1, 3, and 7 days. The cells were stained with FITC-Ghost Pen Cyclic Peptide and DAPI. Human skin fibroblasts, keratinocytes, and HUVECs were added to the matrix patches at a density of 2×10^5 cells/well. Cell adhesion was assessed by counting the cells attached to the matrix patches after incubation in serum-free medium for 4, 6, 8, 12, and 24 h. The adhesion of the cells to the patches was observed.

HUVECs and human skin fibroblasts were lysed using RIPA lysis buffer supplemented with a protease inhibitor cocktail (P8340, Sigma, USA). The wound and surrounding skin tissue were also lysed using RIPA lysis buffer. After suspension in SDS loading buffer and heating at 95 °C for 10 min, 25 μL of the samples were loaded onto an SDS-PAGE gel and electrotransferred to PVDF membranes (E802-01, Vazyme, Vazyme Biotech Co.,Ltd, China). The membranes were blocked with TBST containing 5 % nonfat dry milk at room temperature for 1.5 h, followed by incubation with primary antibodies at the indicated

dilutions overnight at 4 °C. The primary antibodies used were as follows: Ki67 (13180-T48, Sino Biological Inc, China), 1:500; VEGF (ab32152, Abcam, USA), 1:2000; Atp1a2 (ab166888, Abcam, USA), 1:2000; Calm4 (CSB-PA004454GA01HU, Cusabio), 1:1000; Gngb1 (PA5-101543, Invitrogen), 1:1000; GAPDH (#2118S, CST), 1:1000. After incubation with HRP-linked mouse anti-rabbit secondary antibody (#ab99697, Abcam) for 1 h at room temperature, the PVDF membranes were visualized using an ECL chemiluminescence kit (E1050, LabLead, China) and imaged using the TANON 5200 Multi (TANON, Beijing, China).

2.11. Construction of wounds model in diabetic mice

C57BL/6J mice were divided into five groups of six mice each. After one week of acclimatization, the mice were fed a high-fat diet for one week and then intraperitoneally injected with streptozotocin (60 mg/kg) to induce a diabetes model. Mice with blood glucose levels ≥16.8 mmol/L, maintained for two weeks, were considered diabetic and used for subsequent experiments. Prior to wound creation, the mice were injected with the catalase inhibitor 2-amino-1,2,4-triazole (ATZ) at 1 g/kg and allowed to rest for 20–30 min. The dorsal skin of each mouse was sterilized, and a circular wound with an average diameter of 10 mm was created using a skin punch. The wounds were photographed immediately after formation, then topically treated with the glutathione peroxidase inhibitor mercaptosuccinic acid (MSA). After 5 min, the defects were gently wiped with sterile gauze, rinsed with 5 mL of sterile saline, and covered with dressings. Body weight and blood glucose levels were monitored two weeks before and throughout the experiments. This procedure was used to establish a mouse model of difficult-to-heal wounds.

The mice were divided into non-diabetic and diabetic groups. 6 non-diabetic mice in the normal group were not subjected to diabetic model construction. Wounds were prepared as follows: 24 diabetic mice were divided into four groups (n = 6 per group). In the PBS group, wounds were washed with PBS. In the exosomes group, wounds were treated with adipose stem cell-derived exosome suspensions applied to the skin around the wounds. In the bilayer matrix patches group, wounds were covered with bilayer matrix patches that did not contain exosomes. In the exosome-containing bilayer matrix patches group, wounds were covered with bilayer matrix patches that contained exosomes. Wound regeneration was observed on days 0, 3, 7, 10, and 14 after treatment. During the experiment, wounds were treated with exosomes or bilayer matrix patches every two days. At the end of the experiment, the wound area was measured and recorded, and the wound closure index was calculated.

2.12. Intra-tissue delivery efficiency and biodistributions of exosomes

According the previous study's method [26], adding 2 μL of PKH-26 to 500 μL of Diluent C, mix thoroughly by pipetting with 100 μL of ADSCs-Exo at a concentration of 1 μg/μL, and stain at room temperature for 5 min. Add 500 μL of 1 % BSA to stop the staining reaction, then add 10 mL of sterile PBS, centrifuge at 120,000 g for 2 h at 4 °C to remove excess dye. Resuspend the PKH-26-labeled ADSCs-Exo in 100 μL of sterile PBS. Next, load 50 μg of PKH-26-labeled ADSCs-Exo and 50 μg of FITC-labeled liposomes onto a bilayer membrane patch, and transplant it onto the skin defect of diabetic mice. The mice will be sacrificed on days 1, 3, 7, and 14. The liver, kidneys, spleen, and full-thickness skin, extending 5 mm around the wound, will be completely excised, fixed in 4 % paraformaldehyde, embedded in OCT, and sectioned into 5 μm thick frozen sections. The sections will be mounted with anti-fluorescence quenching mounting medium containing DAPI, and observed under a fluorescence microscope for imaging and documentation.

2.13. Antibacterial assay of pericardial decellularized matrix bilayer patch

The disc diffusion test was used to obtain the antibiogram of the pericardial decellularized matrix bilayer patch. This test was performed on both native pericardial tissue and dECM. Staphylococcus aureus was cultured on Müller-Hinton agar, following the method described in a previous study [27]. The native pericardial tissue and dECM were placed in the culture medium using sterile forceps, and the plates were incubated at 37 °C for 24 h. Subsequently, the clear zone of inhibition was measured.

To determine whether the pericardial decellularized matrix bilayer patch exhibits antibacterial effects in vivo, on the days 10, we completely removed the wound from the back of the mice. First, the wound was washed with saline to remove surface impurities and scabs. Then, bacteria from the interior of the wound were extracted using ultrasonic vibration and cultured on Müller-Hinton agar at 37 °C. After 24 h, the number of bacterial colonies from different groups was counted on the culture plates.

2.14. Histology and immunohistochemical staining

The wound area, including the surrounding skin, was collected at 7 and 14 days postoperatively. The samples were fixed in 4 % paraformaldehyde, dehydrated, embedded in paraffin, and cut into 5 μm sections. These sections were stained with hematoxylin and eosin (H&E) and Masson's trichrome according to the manufacturer's instructions. H&E staining was used to assess inflammatory cell infiltration, while Masson's trichrome staining was utilized to evaluate collagen content and maturation in the wound bed. Granulation tissue thickness and epithelial formation length were measured on postoperative days 7 and 14 using image analysis software, and the area positive for collagen synthesis was quantified.

To further examine wound vascularization, blood vessel formation was identified by immunohistochemical staining for CD31. Additionally, to evaluate dECM production and remodeling during the wound healing process, collagen expression was assessed by immunohistochemical staining for collagen III and collagen I. For immunohistochemistry, sections underwent antigen retrieval, followed by overnight incubation with the primary antibody. The sections were then incubated with the secondary antibody for 30 min, stained with diaminobenzidine and hematoxylin, dehydrated, cleared, and sealed.

2.15. RNA sequencing (RNA-seq)

RNA samples from wound skin's cell suspension of three mouse in the PBS group, three in the exosomes group, three in the dECM + collagen group and three in the dECM + collagen + Exo group, were prepared for general transcriptome RNA sequencing data. The RNA samples were extracted by the Trizol method. RNA-seq was performed by PTM BIO Services (Beijing, China). RNA-seq was performed on the Illumina NovaSeq 6000 platform. The edge package in R package DESeq2 was used to screen out the diferently expressed genes with the threshold: p-value <0.05 and Log^2 Fold Change (FC) ≥ 1.

2.16. Western Blotting

The wound and surrounding skin tissue were also lysed using RIPA lysis buffer. After suspension in SDS loading buffer and heating at 95 °C for 10 min, 25 μL of the samples were loaded onto an SDS-PAGE gel and electrotransferred to PVDF membranes (E802-01, Vazyme, Biotech Co., Ltd, China). The membranes were blocked with TBST containing 5 % nonfat dry milk at room temperature for 1.5 h, followed by incubation with primary antibodies at the indicated dilutions overnight at 4 °C. The primary antibodies used were as follows: Atp1a2 (ab166888, Abcam, USA), 1:2000; Calm4 (CSB-PA004454GA01HU, Cusabio), 1:1000;

Gngb1 (PA5-101543, Invitrogen), 1:1000; GAPDH (#2118S, CST), 1:1000. After incubation with HRP-linked mouse anti-rabbit secondary antibody (#ab99697, Abcam) for 1 h at room temperature, the PVDF membranes were visualized using an ECL chemiluminescence kit (E1050, LabLead, China) and imaged using the TANON 5200 Multi (TANON, Beijing, China).

2.17. Immunofluorescence staining

At day 7, the wound were excised to prepared paraffin sections. sections were incubated with Rabbit polyclonal or monoclonal antibodies against CD206 (orb4941, Biorbyt), iNOS (ab283655, Abcam, UK), F4/80 (ab300421, abcam, USA) at 4 °C overnight, and then incubated with species-matched 488-conjugated secondary (#ab150077, abcam, USA), 647-conjugated secondary antibodies (#ab150115, abcam, USA), and the nuclei were counterstained with DAPI at room temperature for 15 min.

2.18. Quantitative real-time polymerase chain reaction (RT-qPCR)

Total RNA was extracted using commercial reagent (AC0205-B, Shandong Sparkjade Biotechnology Co., Ltd). Complementary DNA was reverse-transcribed using a ReverTra Ace qPCR kit (Toyobo, Osaka, Japan). RT-qPCR was performed using TransStart® Tip Green qPCR SuperMix (AG11732, ACCURATE BIOTECHNOLOGY(HUNAN) CO., LTD, ChangSha, China) for the following genes:

cd86, forward 5′-ACGTATTGGAAGGAGATTACAGCT-3′ and reverse 5′-TCTGTCAGCGTTACTATCCCGC-3’;

arg-1, forward 5′-CATTGGCTTGCGAGACGTAGAC-3′ and reverse 5′-GCTGAAGGTCTCTTCCATCACC-3’;

il-6, forward 5′-TACCACTTCACAAGTCGGAGGC-3′ and reverse 5′-CTGCAAGTGCATCATCGTTGTTC-3’;

cd163, forward 5′-GGCTAGACGAAGTCATCTGCAC-3′ and reverse 5′-CTTCGTTGGTCAGCCTCAGAGA-3’; Relative gene expression was normalized to the housekeeping gene glyceraldehyde-3-phosphate dehydrogenase (gapdh) by the $2^{-\Delta\Delta Ct}$ method.

2.19. Statistical analysis

GraphPad Prism v9 (GraphPad Software, San Diego, USA) was used to perform statistical analyses and create graphs. Ordinary one-way ANOVA, including multiple comparison tests, and t-tests were used for statistical analysis. $p < 0.05$ *, $p < 0.01$ ** and $p < 0.001$ *** were considered to be statistically significant, and *ns* represented non-significance.

3. Results

3.1. Characterization and in vitro effect of adipose stem cell exosomes

3.1.1. Characterization of adipose stem cells and their exosomes

The adipose stem cells isolated from the P3 generation using enzymatic digestion were purer and more stable in proliferation, and most of the cells showed a long shuttle shape (Fig. 1A). During the process of induced differentiation of ADSCs to adipocytes, the cells gradually shifted from a long shuttle shape to an ovoid shape, and the number of lipid droplets increased with the prolongation of the incubation time. On the 14 day of induction, these oval-shaped cells were stained red using oil red O staining, confirming that the isolated ADSCs had a propensity to differentiate into adipocytes. ADSCs were also cultured in a chondrogenic differentiation-inducing solution for 21 days. After staining with alcian blue, a typical oval chondrocyte morphology was observed under the microscope, with all cells stained blue, indicating that the isolated ADSCs could also differentiate into chondrocytes. Furthermore, ADSCs were cultured in an osteogenic differentiation induction solution for 21 days. Upon microscopic observation after alizarin red staining, extracellularly deposited calcium nodules were evident, appearing crimson (Fig. 1A), which confirmed that the isolated ADSCs had the potential to differentiate into osteoblasts. These results highlight the multidirectional differentiation potential of the isolated adipose stem cells.

ADSCs of the third generation were selected and the expression of ADSCs surface markers was examined by flow cytometry. The results showed that almost all ADSCs highly expressed MSC markers (CD73, CD166, CD44, with 98.24 %, 98.18 %, and 99.10 %, respectively, while the expression of hematopoietic stem cell markers (CD34, CD14, and CD45) was only 1.60 %, 5.73 %, and 1.14 %, respectively, suggesting that the isolation of the highly pure of ADSCs (Fig. 1B).

Transmission electron microscopy (TEM) of adipose stem cell-derived ADSC-exosomes isolated by ultracentrifugation revealed that the exosome particles had a cup-shaped appearance, exhibited a round vesicle-like structure, and possessed a lipid bilayer membrane (Fig. 1C). Western blot analysis showed significant expression of the transmembrane proteins CD63, CD81, and TSG101 in the exosomes (Fig. 1D). Particle size analysis of the supernatants from ADSC cells indicated that the highest concentration of particles measured 120 nm, with an average particle size of 85 nm and a concentration of 3.2×10^7 particles/mL (Fig. 1E). These findings confirm the high purity of our extracted exosomes.

3.1.2. In vitro effects of adipose stem cell exosomes on fibroblasts, keratinocytes and umbilical vein endothelial cells

The CCK-8 kit was used to assess the effects of different concentrations of exosomes on the proliferative abilities of human skin fibroblasts and keratinocytes at various time points. Concentrations of 30 μg/mL and 50 μg/mL of exosomes demonstrated significant pro-proliferative effects in both fibroblasts (Fig. 2A) and keratinocytes (Fig. 2B). This indicates that higher concentrations (50 μg/mL) of adipose stem cell-derived exosomes have beneficial effects on skin regeneration. In the wound healing process, the migration of fibroblasts and keratinocytes plays a crucial role in determining the healing speed. The pro-migratory effects of different concentrations of exosomes on these two cell types were evaluated using Transwell assays. The results showed that both 30 μg/mL and 50 μg/mL of exosomes significantly promoted the migration of fibroblasts (Fig. 2C and D) and keratinocytes (Fig. 2C and E).

3.2. Preparation and characterization of bilayer patches

3.2.1. Characterization of pericardial decellularized matrix bilayer patches containing adipose stem cell exosomes

The porcine pericardial tissue before decellularization appeared red, while the pericardium after decellularization turned white (Fig. 3A–C). The lower DNA content indicated that the decellularization treatment was more effective. The DNA content test is commonly used to evaluate the degree of decellularization, with a general threshold of ≤50 ng/mg considered indicative of complete decellularization [28]. The DNA content of the pericardium before and after decellularization was assessed using a tissue DNA extraction kit ($n = 3$). Compared to the tissue prior to decellularization, the DNA content after decellularization was significantly reduced, falling below the 50 ng/mg threshold (Fig. 3D). Paraffin sections of H&E-stained porcine pericardium before and after decellularization displayed numerous cellular structures, with blue nuclei and pink cytoplasm alongside fibrous tissue components under the microscope. In contrast, no nuclei were visible in the pericardium after decellularization; however, the fibrous components were well preserved, and the scaffolding structure remained intact. There was no significant difference from natural adipose tissue, aside from the absence of nuclei, indicating that the decellularization treatment was thorough (Fig. 3E).

Matrix patches experience contraction stress during the wound healing process and require appropriate mechanical properties to withstand compressive forces while maintaining structural stability. We

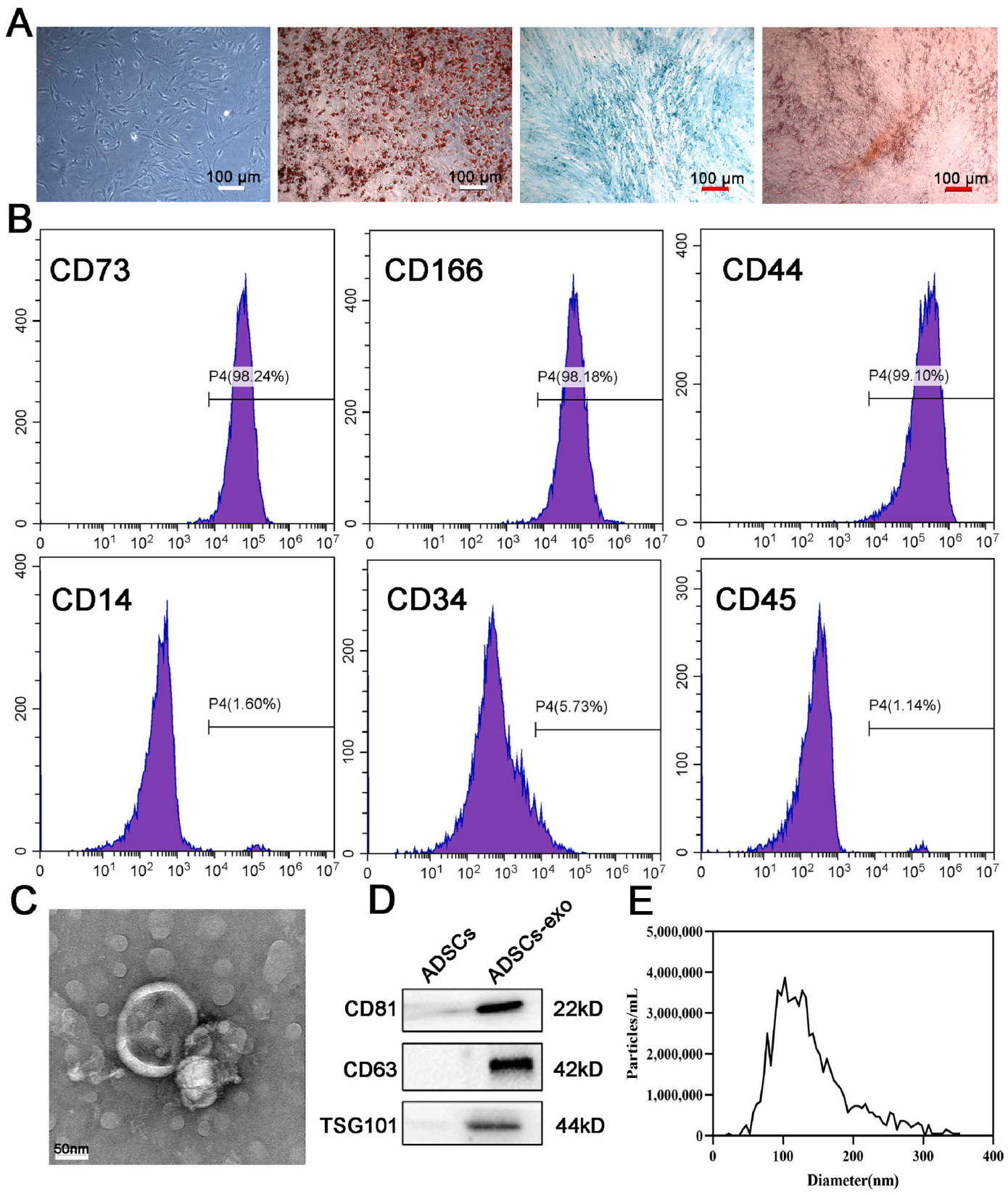

Fig. 1. Characterization of adipose stem cells and their exosomes. (A) morphology of P3 generation adipose-derived stem cells under inverted microscope (left); graph of the results of oil red O staining of adipose stem cells into lipid-induced differentiation (second from left); graph of the results of Alisin blue staining of adipose stem cells into cartilage-induced differentiation (second from right); graph of the results of Alizarin red staining of adipose-derived stem cells into bone-induced differentiation (right). (B) Flow cytometer to identify the expression of adipose-derived stem cell surface markers (CD73, CD166, CD44, CD14, CD34, CD45). (C) Transmission electron microscopy (TEM) photographs of adipose-derived stem cell exosomes; scale bar: 50 nm. (D) Western blot to detect the expression of CD63, CD81, and TSG101 proteins; (E) Nanoparticle tracking analyzer to detect the diameter distribution of adipose stem cell-derived exosomes.

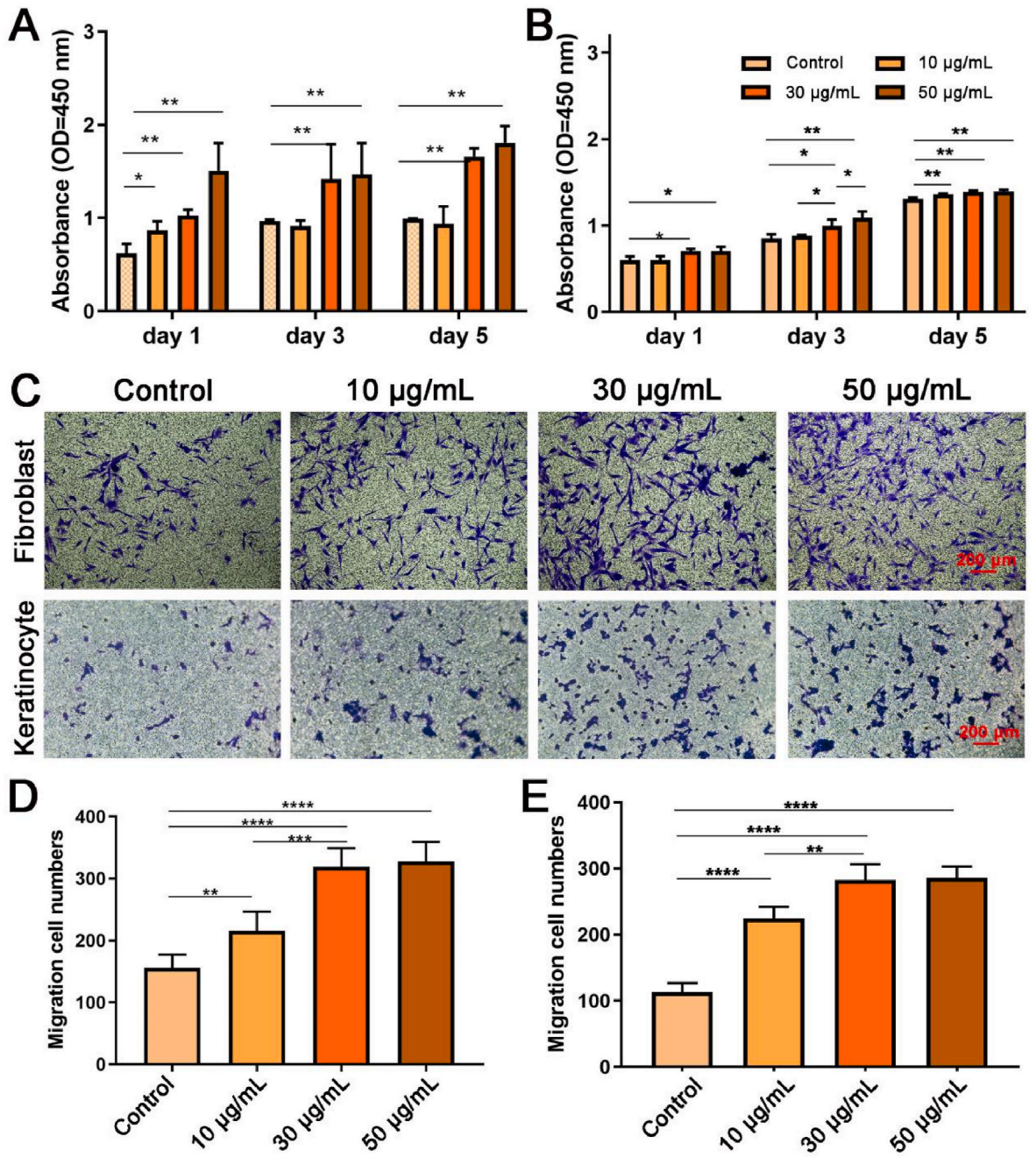

Fig. 2. In vitro effects of adipose-derived stem cell exosomes on fibroblasts, keratinocytes and umbilical vein endothelial cells (HUVEC). (A) CCK-8 results after co-incubation of adipose-derived stem cell exosomes and human skin fibroblasts. (B) CCK-8 results after co-incubation of adipose-derived stem cell exosomes and human skin keratinocyte-forming cells. (C) Images of Transwell experiments in which exosomes promoted the migration of human skin fibroblasts (top) and keratinocytes (bottom); scale bar: 200 μm. (D) statistical analyses of cell migration numbers of fibroblasts, n = 5–6, statistical significance was obtained by one-way ANOVA, **p < 0.01, ***p < 0.001. (E) Statistical analysis of cell migration number of keratinocytes, n = 5, statistical significance was obtained by one-way ANOVA, **p < 0.01, ***p < 0.001.

conducted tensile experiments on single-layer decellularized pericardial membranes and bilayer matrix patches containing collagen, plotting the compression-stress-strain curves (Fig. 3H). The results indicated that the bilayer matrix patches had a lower tensile modulus than the monolayer, but they still exhibited sufficient mechanical properties to inhibit the expansion and contraction of the wound to some extent, thereby providing a favorable mechanical environment for cell attachment and tissue regeneration.

Scanning electron microscopy revealed that the decellularized matrix of the monolayer porcine pericardium exhibited a loose microstructure (Fig. 3F, left). The collagen layer of the bilayer matrix patches, prepared after coating with rat tail collagen, displayed a collagen fiber structure (Fig. 3F, right). The SEM lateral view illustrated the structures of the prepared monolayer and bilayer matrix patches (Fig. 3G). The extracellular matrix formed an interconnected fibrous network, with loosely arranged fibers and non-uniform pore sizes. This structure provides an optimal environment for the migration and growth of fibroblasts and keratinocytes during the wound healing process. Additionally, the collagen fibrous structure of the rat tail collagen layer offers structural support for the attachment of exocytotic cells, and this collagen-rich bilayer structure is conducive to collagen remodeling in the later stages of healing.

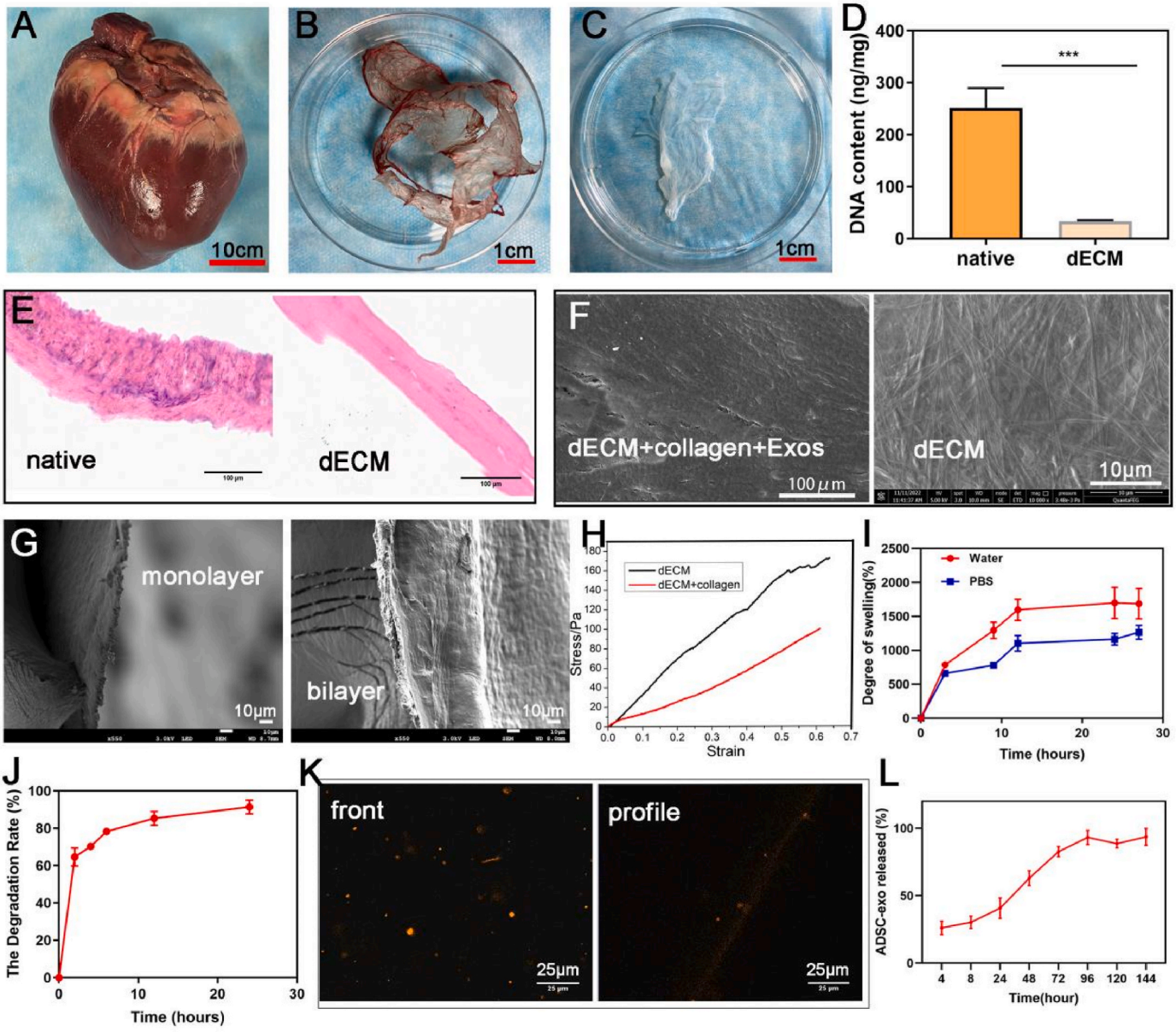

Fig. 3. Characterization of porcine pericardial decellularized matrix (dECM) bilayer patches containing exosomes. (A–C) Diagram of the process of decellularized matrix in isolated porcine pericardium. (D) Comparison of DNA content between porcine pericardium (native) and dECM. (E) H&E staining of native pericardial membranes and decellularized porcine pericardium; (F) SEM picture of monolayer and bilayer decellularized porcine pericardium material (dECM + collagen + Exo). (G) SEM lateral view of dECM and bilayer matrix patches, scale bar: 10 μm. (H) Tensile modulus assay of dECM and bilayer matrix patches. (I) Determination of swelling rate (J) and degradation of bilayer matrix patches in water and PBS (n = 3). (K) Confocal maps of exosome distribution on the surface (left) and profile (right) of bilayer matrix patches, scale bar: 25 μm. (L) Exosomes releasing rate from the bilayer matrix patches (n = 3).

The water absorption of the bilayer matrix patches at 0, 3, 9, 12, 24, and 27 h was examined. The results of the dissolution rate experiments are presented in the figure (Fig. 3I). It can be observed that the swelling rate of the bilayer matrix patches in both water and PBS increased rapidly during the first 3 h, reaching swelling equilibrium at approximately 12 h, with better performance in water. This indicates that the bilayer matrix patches have superior moisturizing properties, making them ideal for use as wound dressings. Collagenase I is an important degrading enzyme in the skin. The weight loss of the bilayer matrix patches soaked in 50 mg/mL collagenase I is shown in the graph (Fig. 3J). The degradation rate is faster during the initial 2 h and then slows down, which may be related to the rapid degradation of the collagen layer. The bilayer matrix patches can be completely degraded within 24 h, demonstrating their effectiveness as a biomaterial.

Exosomes, as an important component of the wound dressing in this study, play a crucial role in determining the effectiveness of wound treatment through their encapsulation and release efficiency. The double-layer matrix patches were prepared after exosome encapsulation, and their distribution was observed using confocal microscopy (Fig. 3K). The results showed that a large number of exosomes were distributed within the collagen layer of the double-layer matrix patches. To assess in vitro release, the exosome-containing bilayer matrix patches were immersed in PBS, and the results are presented in the figure (Fig. 3L). The exosomes in the matrix patches reached equilibrium in their in vitro release within 100 h, indicating that the exosomes encapsulated in the patches can be released continuously to play a therapeutic role during the inflammatory stage of wound healing.

3.2.2. Cellular effects of porcine pericardial decellularized matrix bilayer patches containing adipose stem cell exosomes

To assess cell growth and adhesion on the bilayer matrix patches, human skin fibroblasts, keratinocytes, and umbilical vein endothelial cells were inoculated onto the patches and cultured separately. Confocal microscopy (Fig. 4A) revealed that all three cell types maintained normal growth morphology on the patches, with an increasing cell count (Fig. 4B). This promotes the proliferation of cells that migrate during the wound healing process, reflecting the good biocompatibility of the bilayer matrix patches.

The migration of fibroblasts was enhanced when both factors (exosomes and the porcine pericardial decellularized matrix) were present together. Further Western blot experiments showed that the Ki67 protein level was highest in the dECM + collagen + Exo group. Ki67 is an indicator of cell proliferation and migration rates (Fig. 4C and F). Cardiac-derived matrices have been shown to have favorable pro-angiogenic effects [29]. To verify the angiogenic effect of the pericardial decellularized matrix, an in vitro tubule formation assay was conducted using umbilical vein endothelial cells with extracts from the matrix patches. The results from both the tubule formation assay and Western blot analysis indicated that the culture medium containing the decellularized matrix could also promote tubule formation in umbilical vein endothelial cells (Fig. 4D–F).

3.2.3. Antibacterial assay of pericardial decellularized matrix bilayer patch in vitro

To verify whether dECM + collagen + Exo has antibacterial properties in vitro, we co-cultured dECM + collagen + Exo with *Staphylococcus aureus* (a common pathogen in chronic wounds), using native pericardial tissue as a control. As shown in Fig. S1, no significant inhibition zone was observed around either material, suggesting that dECM + collagen + Exo does not inhibit the proliferation of *Staphylococcus aureus* in vitro.

3.3. Treatment of diabetic wounds in mice

3.3.1. Treatment of diabetic wounds in mice

The healing of wounds in mice reflects the healing-promoting ability of wound dressings. Statistics on the wound area at different time points (Fig. 5A) revealed that the wounds of mice in the Normal group (without diabetic model construction) healed significantly within 14 days. In contrast, the wounds of diabetic mice in the PBS group were more challenging to heal. The addition of exosome drops (Exosomes) promoted a reduction in the wound area of the mice. Furthermore, the wounds of mice treated with the double-layer matrix patches (dECM + collagen group) also healed significantly compared to the PBS group. When both factors were present (dECM + collagen + Exo group), wound healing in the mice approached normalization, achieving healing effects similar to those observed in the Normal group (Fig. 5B).

3.3.2. H&E staining

H&E staining was used to assess the effects of granulation tissue and epithelialization at the healing site. After 7 days, all groups exhibited signs of healing. The skin at the wounds of the dECM + collagen-treated mice demonstrated effective granulation tissue regeneration and re-epithelialization. The addition of exosomes significantly enhanced tissue regeneration. After 14 days, the wounds in the Normal group and the group treated with double-layer matrix patches containing exosomes were nearly closed (Fig. 6A). Furthermore, granulation tissue regeneration (Fig. 6B) and epithelial thickness (Fig. 6C) were superior in these groups compared to the others.

3.3.3. Masson staining

Masson staining was conducted to detect the retention of collagen components in skin tissue, with results shown in Fig. 7A. In the PBS group, collagen fibers in the skin tissue appeared loose. In contrast, the groups treated with exosomes or patches displayed blue-stained, aligned collagen fibers. Notably, in the dECM + collagen + Exo group, collagen fibers were intact and tightly aligned, indicating a strong collagen regeneration effect. Statistical analysis of the positive area from Masson staining revealed that the double-layer matrix patches-treated group had a significantly larger positive area, suggesting that exosomes and double-layer matrix patches effectively promote collagen synthesis in treated wounds (Fig. 7B).

3.3.4. Immunohistochemical staining

CD31, also known as platelet-endothelial cell adhesion molecule, is primarily used to identify the presence of endothelial cells and assess tissue angiogenesis [30]. Vascular regeneration in the skin directly influences healing speed and outcomes. Immunohistochemical staining of mouse skin at the healing site was conducted at 7 and 14 days for CD31, along with statistical analysis of the number of angiogenic events (Fig. 8A). The results showed that both the exosome and bilayer matrix patch groups promoted CD31 expression. Notably, the expression in the dECM + collagen + Exo group was significantly higher than in the other groups (Fig. 8B), indicating that bilayer matrix patches containing exosomes effectively promote angiogenesis during the healing process.

Collagen type I (COL 1) is thicker and provides support for skin stiffness. However, excessive amounts can lead to scar formation after wound healing (Fig. 8C). In contrast, collagen type III (COL 3) is thinner and contributes to skin suppleness, making the skin delicate and elastic (Fig. 8D and E). The ratio of COL 3 to COL 1 reflects the quality of skin healing and influences scar formation. Immunohistochemical staining of both collagen types indicated an increase in the dECM + collagen + Exo treatment group, with particularly high expression of COL 3 promoting skin healing and inhibiting scar formation (Fig. 8F).

3.3.5. Antibacterial assay of pericardial decellularized matrix bilayer patch in vivo

The antibacterial properties of the material can help prevent the formation of biofilms by bacteria in the wound, which is a key factor in the persistence of hard-to-heal wounds. To verify whether dECM + collagen + Exo inhibits bacterial proliferation in vivo, we collected bacteria from the wounds of different treatment groups and cultured them in vitro for 24 h. The number of bacterial colonies formed on the surface of the culture medium reflected the number of bacteria present in the wounds of different treatment groups. As shown in Fig. S2, the number of bacterial colonies in the dECM + collagen group and dECM + collagen + Exo group was significantly reduced compared to the PBS group, indicating that the decellularized pericardial matrix material has a certain antibacterial effect in vivo. Considering the in vitro antibacterial test results (dECM + collagen + Exo did not inhibit bacterial proliferation), we speculate that dECM may exert its antibacterial effect by activating the immune system in vivo.

3.3.6. Intra-tissue delivery efficiency and biodistributions of exosomes

To explore the intra-tissue delivery efficiency of exosomes, we first loaded PKH26-labeled ADSCs-Exo onto the dECM and then transplanted it into the skin wounds of diabetic mice. We observed the localization of the ADSCs-Exo using immunofluorescence microscopy at 1, 3, 7, and 14 days post-transplantation. As shown in Fig. S3, on day 1, the exosomes were confined to the dermis layer, and by day 3, exosomes were observed below the dermis layer. The maximum concentration and depth of exosome delivery were reached on day 7, with exosomes even appearing in the muscle tissue. Over time, the exosome content in the subdermal layer gradually decreased, but significant exosome presence was still observed within the dermis layer (on day 14).

Additionally, by comparing the duration of ADSCs-Exo with other lipid nanoparticles (LNPs), especially those already used in clinical settings, we can explore the translational potential of ADSCs-Exo further. We loaded an equal amount of FITC-labeled commercially available liposomes into the decellularized pericardium and then

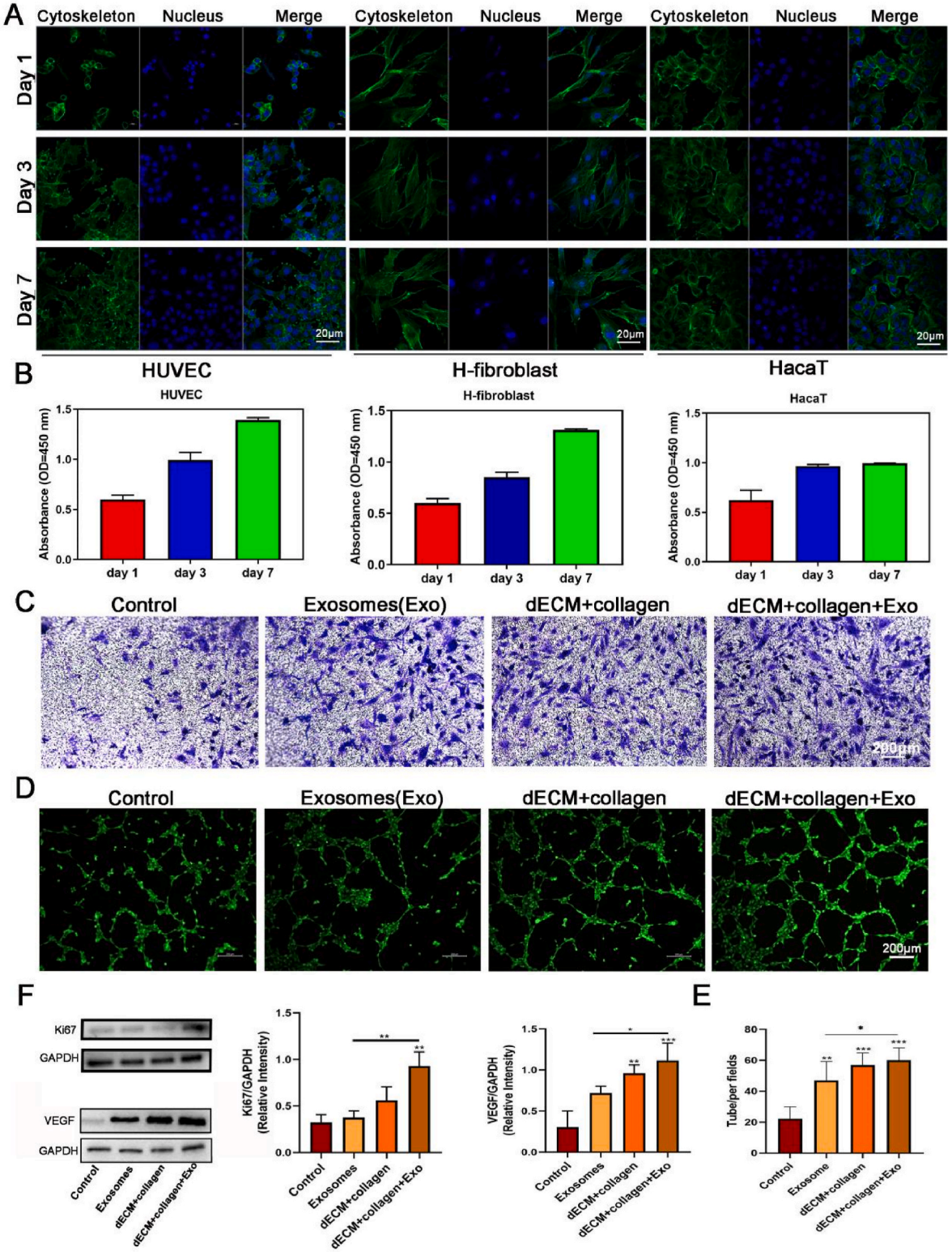

Fig. 4. Effects of porcine pericardial decellularized matrix bilayer patches containing exosomes (dECM + collagen + Exo) on cells in vitro. (A) Morphological observations of three cell types after 1, 3, and 7 days of growth on the surface of bilayer matrix patches, (green: cytoskeleton, blue: DAPI). (B) Cells' viability after co-incubation of dECM + collagen + Exo and human skin fibroblasts, keratinocytes and HUVEC. (C) Transwell images of human skin fibroblasts when co-cultured with dECM + collagen + Exo bilayer patches. (D) dECM + collagen + Exo bilayer patches induced HUVEC formation tubes. (E) Statistical analysis with tube-forming branches (n = 5). (F) Western Blott evaluation of proliferation-related proteins (Ki67) and angiopoiesis-related proteins (VEGF) expressed by fibroblasts and HUVEC, respectively, n = 3, statistical significance was obtained by one-way ANOVA, *p < 0.05, **p < 0.01, ***p < 0.001.

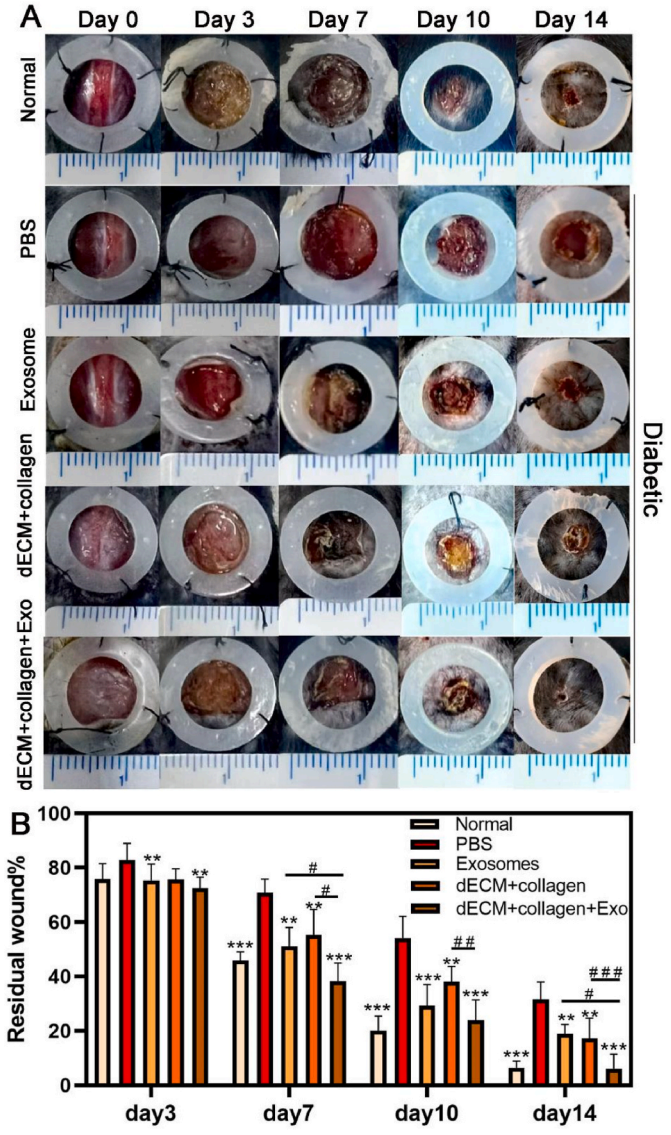

Fig. 5. Wound healing images and statistical analysis of mice in each group after treatment. (A) Gross view of each group' wound on day 3, 7, 10 and 14. (B) Wound area of each group on day 3, 7, 10 and 14, n = 6, statistical significance was obtained by one-way ANOVA, $^{**}p < 0.01$, $^{***}p < 0.001$, compared with PBS group, while $^{\#}p < 0.05$, $^{\#\#}p < 0.01$, $^{\#\#\#}p < 0.001$, compared with dECM + collagen + Exo group.

transplanted it onto the skin wounds of diabetic mice. We observed the localization of green fluorescence using immunofluorescence microscopy at 1, 3, 7, and 14 days post-transplantation. Additionally, to clarify the in vivo distribution of ADSCs-Exo and liposome, we collected the liver, kidneys, and spleen from both groups of animals to determine the distribution of ADSCs-Exo and liposome in these organs at different time points. As shown in Fig. S3, the distribution of liposome in the wound skin peaked on day 3. Starting from day 7, the FITC fluorescence intensity in the skin gradually decreased, and by day 14, liposome were virtually undetectable in the wound skin. Combined with the distribution of ADSCs-Exo in the skin on day 14, these results suggest that the decellularized pericardium has the ability to slowly release ADSCs-Exo. The use of the decellularized pericardium for exosome release to the wound may increase the bioavailability of the exosomes, possibly because ADSCs-Exo can bind to the collagen within the decellularized pericardium matrix, while liposomes cannot.

Moreover, we observed the distribution of the two LNPs in vivo, as shown in Fig. S3. Throughout the treatment period (14 days), ADSCs-Exo were distributed in the spleen, liver, and kidney, indicating that the body can clear ADSCs-Exo through these organs. However, liposomes were only detected in the kidneys on day 3, and in the liver and spleen on day 7. By day 14, liposomes were no longer detectable in the kidney, spleen, and liver tissues. This suggests that liposomes may be primarily cleared through the kidneys, with the clearance efficiency of the kidneys surpassing that of ADSCs-Exo. From a biosafety perspective, rapid clearance from the body may indicate reduced harm to the organism, reflecting a higher safety profile for the biomaterials.

3.4. Mechanisms of decellularized pericardial membrane bilayer patches promote wound healing

To further clarify the potential biological mechanisms by which decellularized pericardial membrane bilayer patches promote the healing of refractory diabetic wounds, we conducted conventional transcriptome sequencing on wound tissue (including the wound and 5 mm of surrounding skin) on the days 7 of treatment with different materials. By comparing the transcriptome data with the PBS group, we identified differentially expressed genes in the other three groups, followed by gene ontology (GO) and Kyoto Encyclopedia of Genes and Genomes (KEGG) analyses of these genes, as shown in Fig. 9.

Fig. 9A presents the volcano plot of differentially expressed genes in the exosomes group, totaling 17,439 differentially expressed genes. The GO analysis in Fig. 9B indicates that the main biological processes (BP) include "chemotaxis", "leukocyte migration", and "immune system activation", as well as biological processes related to "epidermis development" and "skin development" associated with skin regeneration. The most prominent cellular component (CC) is the "collagen-containing extracellular matrix", while molecular functions (MF) such as "extracellular matrix structural constituent" and "glycosaminoglycan binding" are related to extracellular matrix formation. Additionally, KEGG analysis (Fig. 9C) reveals that during the process of exosome-enhanced wound healing, signaling pathways such as the "PI3K-Akt signaling pathway", "Rap1 signaling pathway", and "MAPK signaling pathway" are activated. Previous research has demonstrated that exosomes can promote wound healing by increasing the expression levels of proteins such as ANG1, FILK1, and VEGF, thereby activating the Akt signaling pathway [31] and reducing ROS levels in wounds under high-glucose conditions [31]. Other studies have also found that exosomes can deliver miR-144-3p, linc00511, and miR-106a-5p to activate the MAPK signaling pathway, promoting angiogenesis of endothelial cells in the wound and ultimately accelerating wound healing [32].

Fig. 9D–F illustrate the differentially expressed genes and GO and KEGG analyses in the dECM + collagen group. The GO analysis in Fig. 9E indicates that the main biological processes (BP) include those related to immune system activation, such as "leukocyte migration", "leukocyte cell-cell adhesion", "regulation of inflammatory response", and "cell chemotaxis", as well as biological processes related to skin regeneration, including "epidermis development", "epidermal cell differentiation", and "skin development". The most prominent cellular component (CC) is also the "collagen-containing extracellular matrix". Molecular functions (MF) such as "immune receptor activity", "structural constituent of skin epidermis", and "glycosaminoglycan binding" are associated with immune system activation and extracellular matrix formation. KEGG analysis (Fig. 9F) shows the activation of signaling pathways such as the "NF-kappa B signaling pathway", "IL-17 signaling pathway", and "TNF signaling pathway", which are classic pathways involved in immune activation and other biological processes. Although there is currently no research exploring the potential molecular mechanisms of decellularized pericardial membrane in wound treatment, our results suggest that future research on molecular mechanisms could focus on these signaling pathways.

Fig. 9G–I illustrate the differentially expressed genes and GO and KEGG analyses in the dECM + collagen + Exo group. The GO analysis in

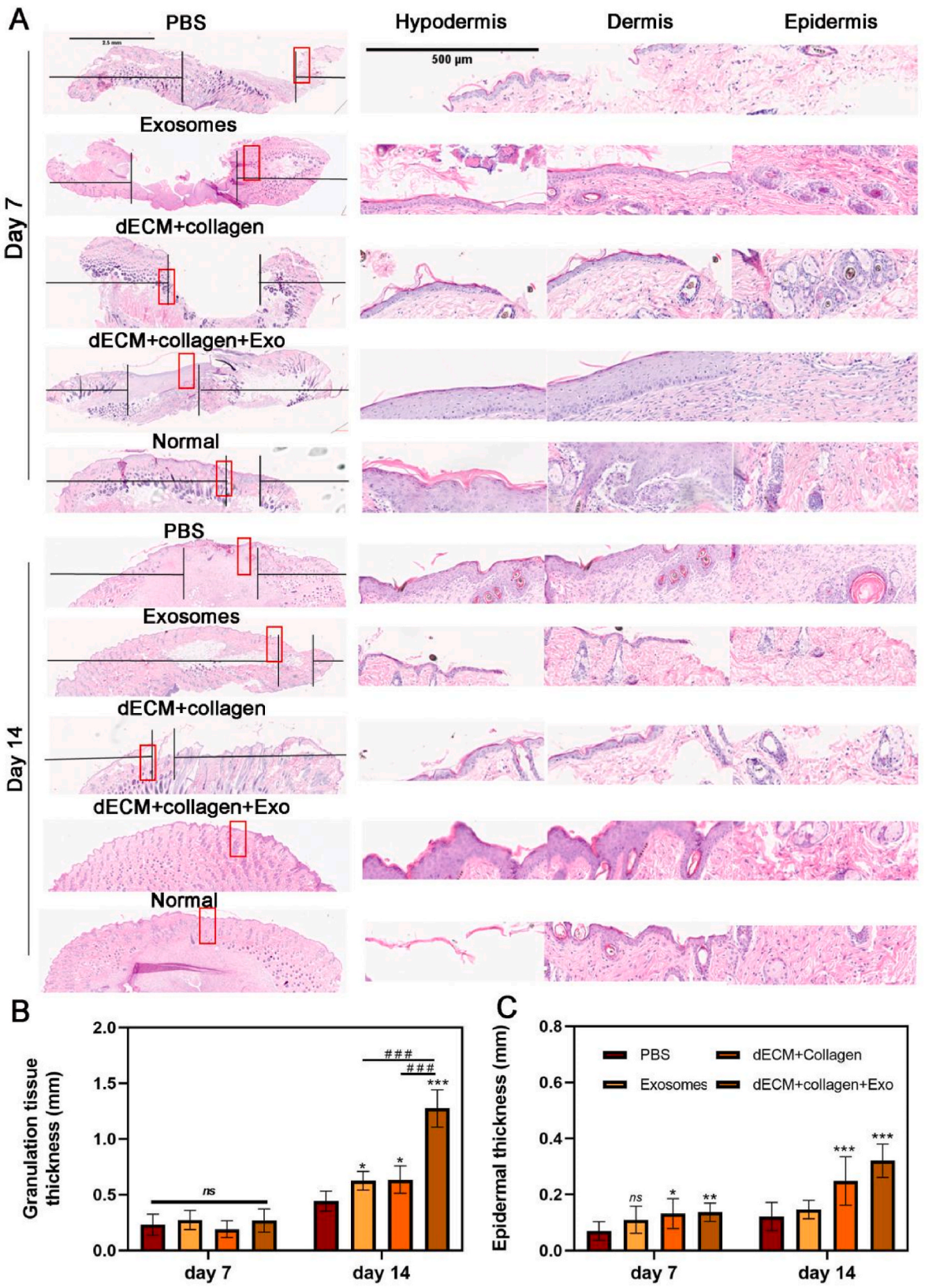

Fig. 6. Statistical results of re-epithelialization and granulation tissue and epithelial thickness of mouse skin assessed by H&E staining. (A) H&E staining of the skin at the healing site at 7 and 14 days after treatment in each group of mice. (B) Statistical analysis of granulation tissue and (C) epithelial thickness based on H&E staining results, (n = 5), *p < 0.05, **p < 0.01, ***p < 0.001, *n.s.* = not significant, compared with PBS group, while $^{###}$p < 0.001, compared with dECM + collagen + Exo group.

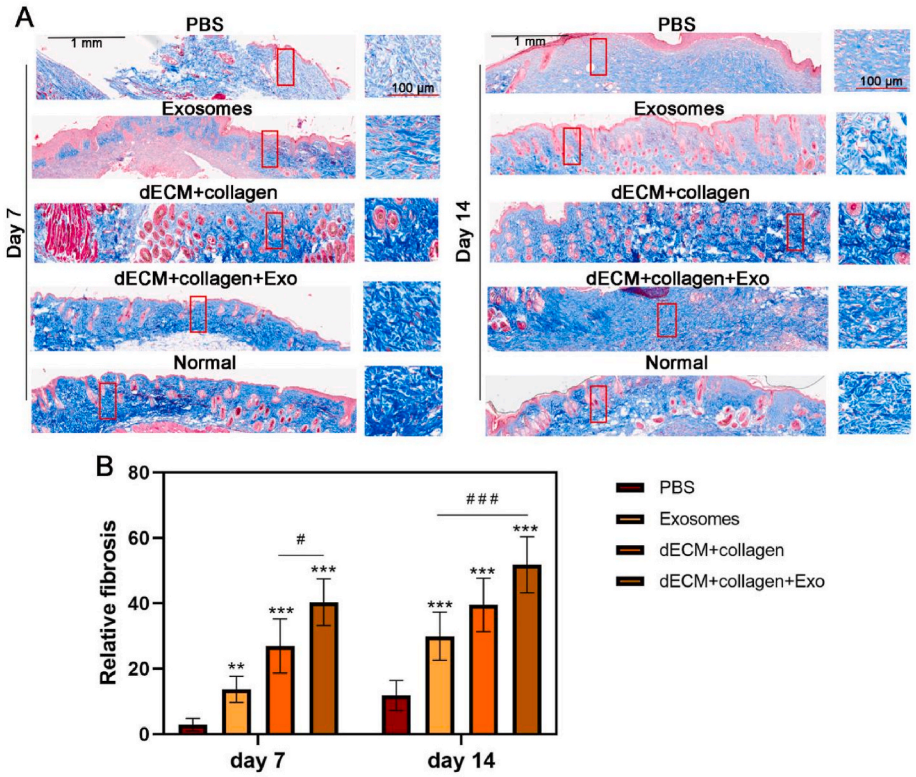

Fig. 7. Masson staining to assess the effect of collagen synthesis in mice skin. (A) Masson staining of the skin at the healing site at 7 and 14 days after treatment in each group of mice. (B) Statistical analysis of collagen deposition based on Masson staining results, (n = 5), $^{**}p < 0.01$, $^{***}p < 0.001$, compared with PBS group, while $^{\#\#\#}p < 0.001$, compared with dECM + collagen + Exo group.

Fig. 9H shows that the main biological processes (BP) include those related to immune system activation, such as chemotaxis, leukocyte migration, and cell chemotaxis, as well as biological processes associated with skin regeneration and vascular formation, such as "extracellular structure organization", "regulation of angiogenesis", and "vascular process in the circulatory system". The most prominent cellular component (CC) is "collagen-containing extracellular matrix". Molecular functions (MF) such as "extracellular matrix structural constituent" and "glycosaminoglycan binding" are related to extracellular matrix formation. KEGG analysis shows the activation of pathways such as "Cytokine-cytokine receptor interaction", "Calcium signaling pathway", "cAMP signaling pathway", and "PI3K-Akt signaling pathway" (Fig. 9I). Previous studies have reported that the PI3K-Akt signaling pathway is a key pathway through which exosomes reduce ROS levels in the wound microenvironment, preventing cell apoptosis. In addition, the Cytokine-cytokine receptor interaction, Calcium signaling pathway, and cAMP signaling pathway have not been previously reported, which may suggest a potential biological mechanism by which the decellularized pericardial membrane loaded with adipose-derived stem cell exosomes promotes wound repair. This mechanism might differ from the biological mechanisms by which exosomes or decellularized pericardial membrane alone promote wound healing.

To reveal the biological mechanisms by which exosome-loaded bilayer patches promote the healing of refractory wounds, we combined the analysis results from the RNA-seq data (Fig. 9). First, we conducted phenotypic identification of macrophages in the wound and surrounding skin tissue on day 7 across all groups (as reported in the literature [33,34], the active time window for macrophages during tissue repair is approximately one week); Therefore, we chose day 7 as the time point for our study to clarify how the biomaterials regulate the local immune microenvironment. The results are shown in Fig. 10A, where we used F4/80 (green fluorescence) as a marker for M0 macrophages, and iNOS (green fluorescence) and CD206 (green fluorescence) as markers for M1 and M2 macrophages, respectively. For M1 macrophages, higher fluorescence intensity of iNOS was observed in the PBS and Exosome groups, while the average fluorescence intensity of iNOS significantly decreased in the dECM + collagen group, a trend that was more pronounced in the dECM + collagen + Exo group. Conversely, the CD206 red fluorescence intensity was low in the PBS and Exosome groups, gradually increasing in the dECM + collagen group, with the highest expression level in the dECM + collagen + Exo group (Fig. 10A). These results indicate that the bilayer patch material can modulate the polarization of macrophages from M1 to M2 in the local microenvironment. Generally, M1 macrophages are pro-inflammatory, while M2 macrophages are anti-inflammatory, and multiple studies have shown that M2 macrophages significantly promote the repair of various tissues [35]. Next, we also assessed the gene transcription levels of cytokines secreted by different macrophages in the tissue to further confirm the important role of macrophages in wound healing. The results, shown in Fig. 10B, from RT-qPCR experiments indicated that in the dECM + collagen + Exo group, the expression levels of M1 macrophage-related genes (*cd86*, *il-6*) were the lowest, showing a significant statistical difference compared to the PBS group. In contrast, the expression levels of M2 macrophage-related genes (*cd163*, *arg-1*) were significantly increased in the dECM + collagen + Exo group, suggesting that activated M2 macrophages play a crucial role in the wound healing process.

Furthermore, based on the GO and KEGG analysis results from the RNA-seq data (Fig. 9), after excluding the overlapping signaling pathways and biological processes associated with the Exosome and dECM + collagen groups, we ultimately focused on the cAMP signaling pathway (Fig. 9I). To verify the activation of this signaling pathway during the healing process facilitated by the bilayer patches, we first determined the expression levels of genes such as Atp1a2, Calm4, and Cngb1 in the RNA-seq data (Atp1a2, Calm4, and Cngb1 are key participants in the cAMP signaling pathway [36]). We then extracted proteins from the wound and surrounding skin, using Western Blotting to further clarify

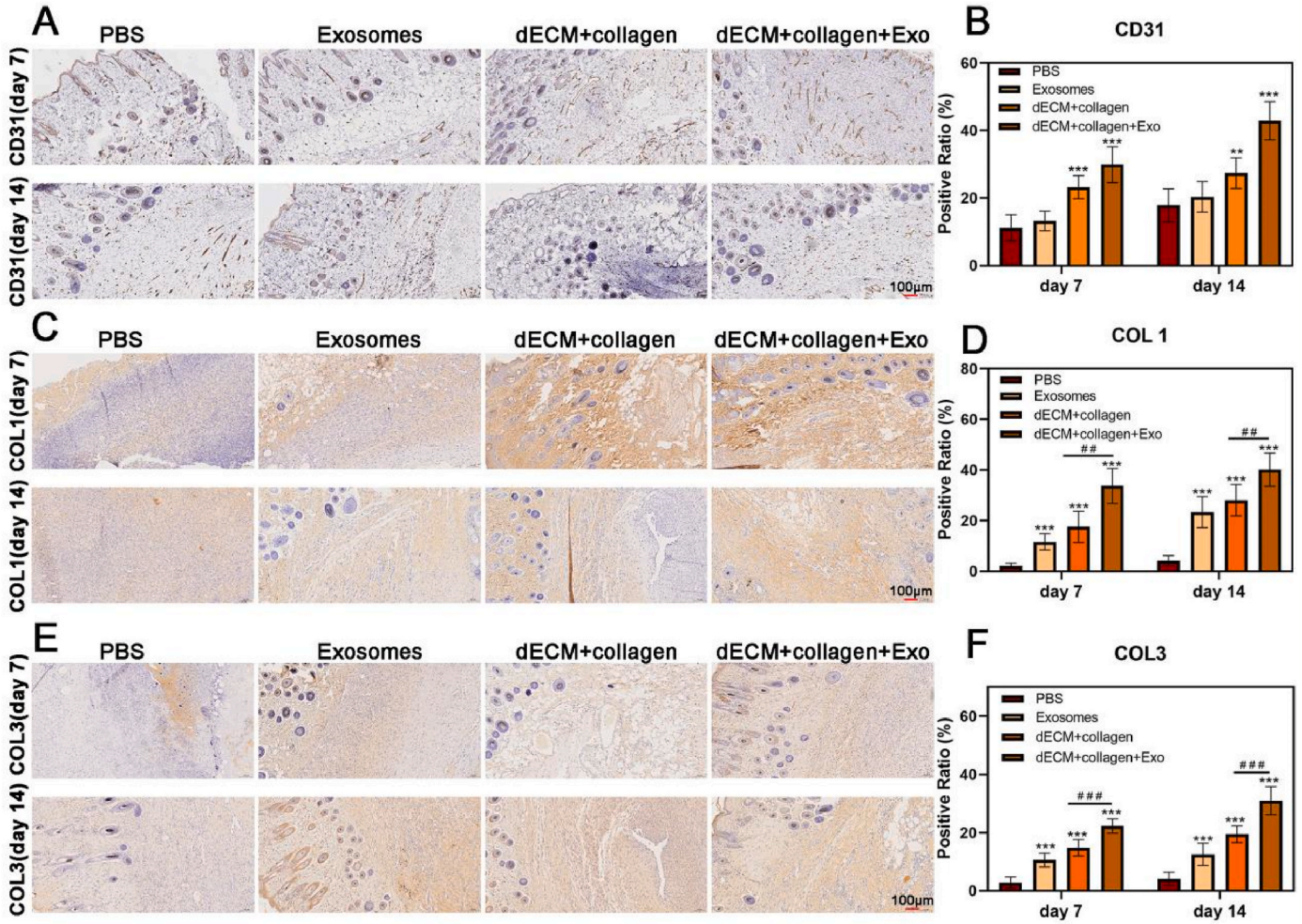

Fig. 8. Immunohistochemical staining results of wound skin tissue. (A) CD31 immunohistochemical staining for assessing angiogenesis in wounds; (B) Statistics on the number of blood vessels; (C) Immunohistochemical staining of COL 1 and statistical analysis of positive area (D), n = 6. (E) Immunohistochemical staining of COL 3 and statistical analysis of positive area (F), n = 6, $^{**}p < 0.01$, $^{***}p < 0.001$, compared with PBS group, while $^{\#\#}p < 0.01$, $^{\#\#\#}p < 0.001$, compared with dECM + collagen + Exo group.

the protein expression levels of Atp1a2, Calm4, and Cngb1 to confirm whether the cAMP signaling pathway was activated and involved in the wound repair process. The Western Blotting results are shown in Fig. 10C and D. Compared to the expression levels of Atp1a2, Calm4, and Cngb1 proteins in the PBS group, there was a slight increase in the Exosome and dECM + collagen groups, but no statistical significance was observed (except for Cngb1 in the dECM + collagen group). In contrast, the expression levels of Atp1a2, Calm4, and Cngb1 proteins in the dECM + collagen + Exo group were significantly elevated, higher than in all other groups, with significant statistical differences (Fig. 10D). This result suggests that the cAMP signaling pathway was indeed activated during the process of wound repair facilitated by the bilayer patches and played a significant role.

In summary, we have revealed that exosome-loaded decellularized pericardial bilayer patches may participate in the repair process of refractory wounds by modulating the polarization of M2 macrophages in the local microenvironment and activating the cAMP signaling pathway. However, we are currently unable to determine whether the activation of the cAMP signaling pathway is related to the activation of M2 macrophages. While some studies have demonstrated that the activation of M2 macrophages is mediated through the cAMP signaling pathway under other disease or cell culture conditions [37], the relationship between these two factors requires further investigation in our experiments.

4. Discussion

Currently, the potential application of adipose-derived stem cell exosomes in the field of wound healing has been extensively explored [38]. However, a current challenge is the low efficiency of local exosome delivery, making it difficult to fully leverage their therapeutic effect on non-healing wounds [9]. To address this, researchers have indeed developed various biomaterials for delivering exosomes to improve their therapeutic efficacy on wounds [39], such as dermal matrices, synthetic hydrogels, and other ECM-based materials. The vast majority of these delivery materials are presented in the form of hydrogels. For example, both simple dermal matrix hydrogels and other ECM-based hydrogels exhibit high exosome loading rates. However, due to the rapid degradation rate of ECM-based hydrogels in vivo, along with their low shear resistance, this inevitably leads to the release of loaded exosomes within a short period, preventing maximum utilization of the exosomes [40]. Furthermore, although some studies have applied other methods for delivering exosomes to wounds, such as microneedles, the process of fabricating microneedles often requires the addition of other substances to enhance their mechanical strength, with GalMA being a common example. The introduction of such materials can inadvertently increase the local immune response at the wound site, which may be detrimental to wound healing [41]. In this study, we developed bilayer patches composed of collagen derived from adipose stem cell exosomes and

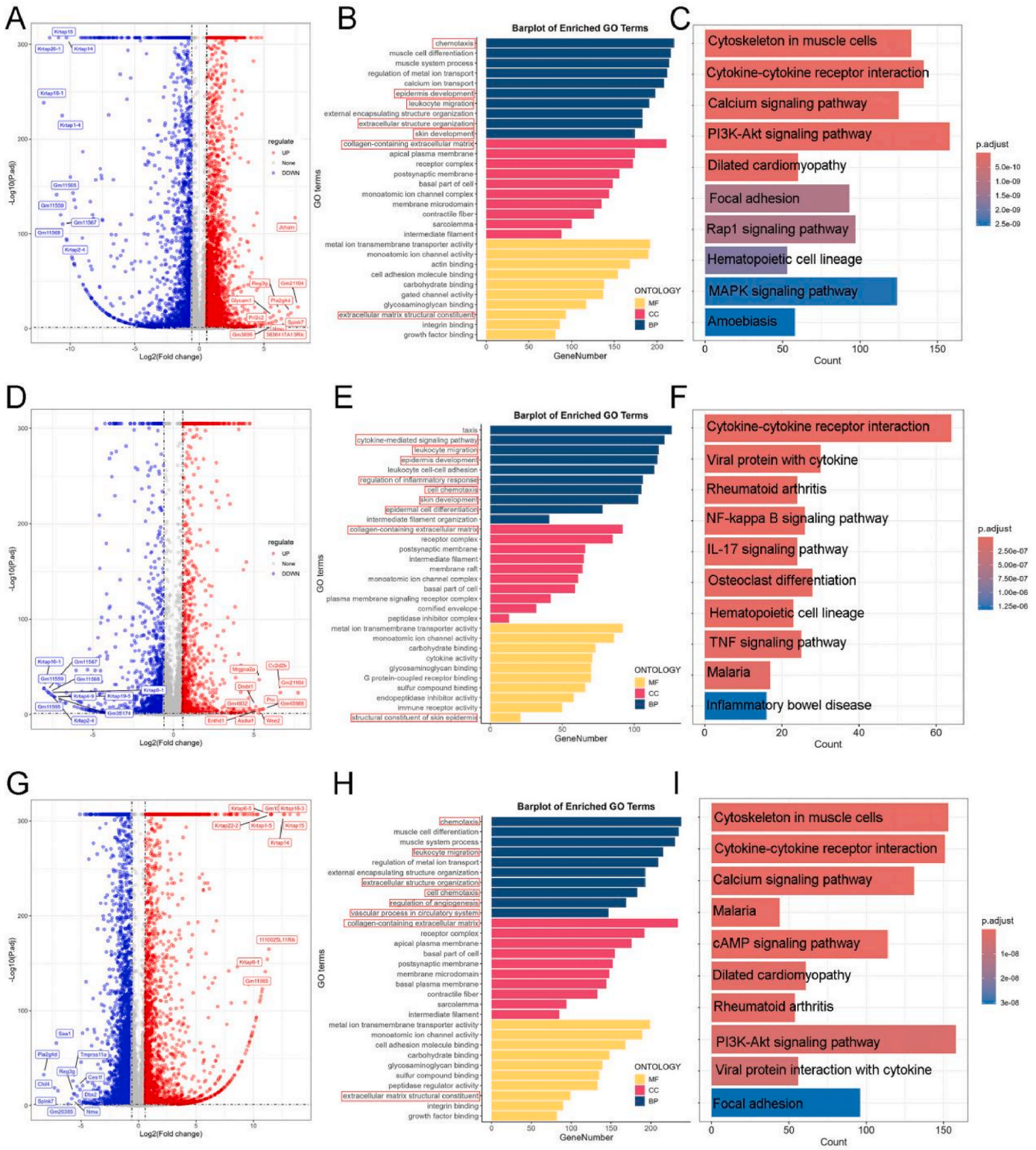

Fig. 9. Mechanisms of decellularized pericardial membrane bilayer patches promote wound healing. (A) Volcano plot of differentially expressed genes (DEGs) in exosomes group. (B) Top-ranked biological processes (BP), cellular component (CC), Molecular functions (MF) revealed through GO analysis in exosomes group. (C) The Top-ranked signal pathway analyzed by the KEGG platform in exosomes group. (D) Volcano plot of DEGs in dECM + collagen group. (E) Top-ranked BP, CC, MF revealed through GO analysis in dECM + collagen group. (F) The Top-ranked signal pathway analyzed by the KEGG platform in dECM + collagen group. (G) Volcano plot of DEGs in dECM + collagen + Exo group. (H) Top-ranked BP, CC, MF revealed through GO analysis in dECM + collagen + Exo group. (I) The Top-ranked signal pathway analyzed by the KEGG platform in dECM + collagen + Exo group.

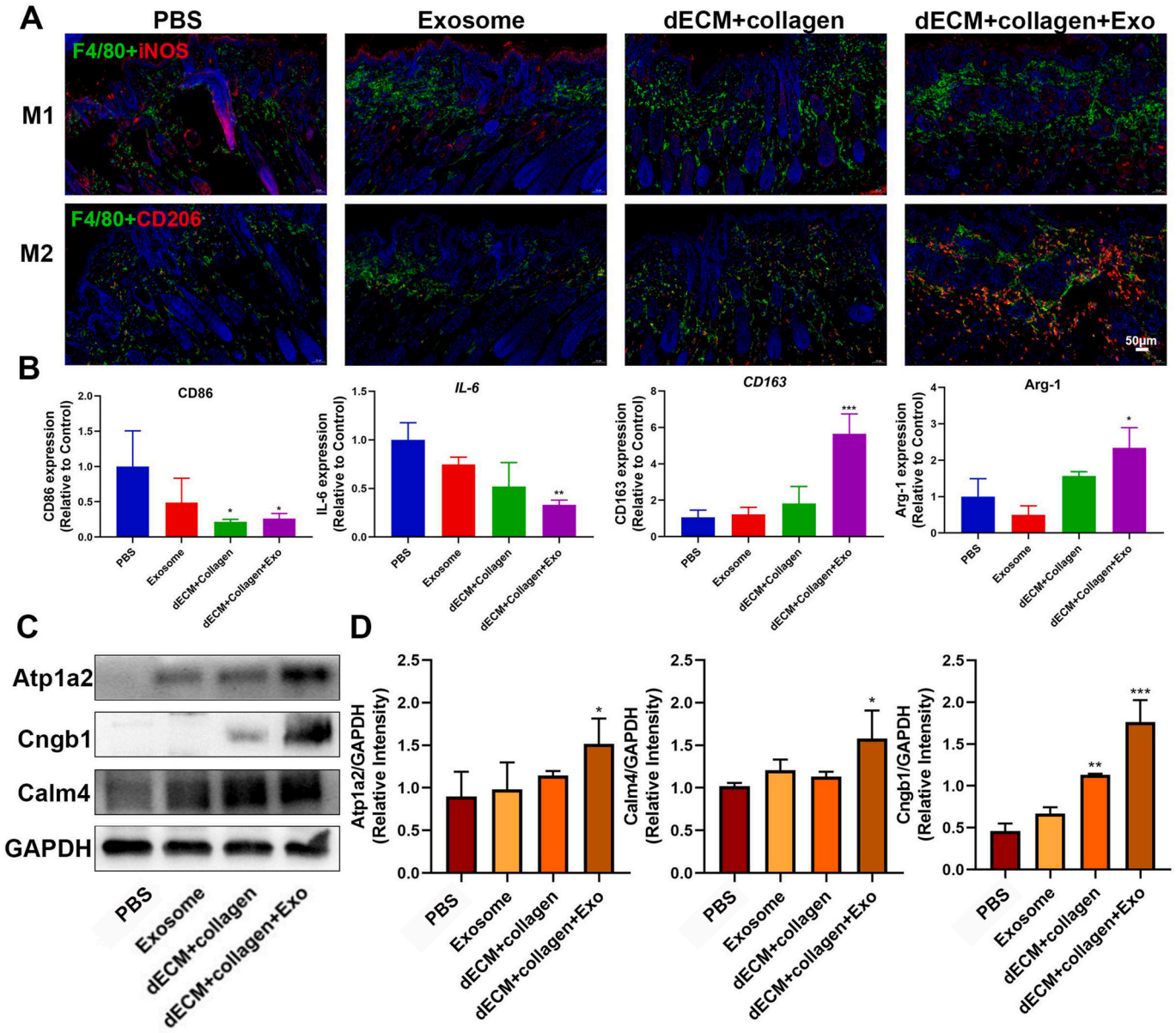

Fig. 10. The exosome-loaded bilayer decellularized pericardial patches promote the healing of diabetic refractory wounds by enhancing the activation of M2 macrophages in the wound and activating the cAMP signaling pathway. (A) On day 7, dual immunofluorescence staining for F4/80 (M0 marker), iNOS (M1 marker), and CD206 (M2 marker) was performed to assess the numbers of activated M1 and M2 macrophages in the wound and surrounding skin tissue, scale bar = 50 μm. (B) On day 7, RT-qPCR was used to detect the expression levels of M1 (*cd86*, *il-6*) and M2 (*cd163*, *arg-1*) macrophage-related genes in the wound tissue of each group. (C) On day 7, Western Blotting experiments were conducted to measure the expression levels of key proteins in the cAMP signaling pathway (Atp1a2, Calm4, and Cngb1) in the wound tissue of each group, with quantitative analysis of protein density, n = 3 (D). *, $p < 0.05$, **, $p < 0.01$, and ***, $p < 0.001$, compared with the PBS group.

porcine pericardial decellularized matrix to investigate their therapeutic effects on skin regeneration-related cells and wounds in diabetic mice. This work provides a reference for utilizing related biomaterials to enhance the treatment of difficult-to-heal wounds.

In recent years, researchers have attempted to use decellularized matrix scaffolds in non-hydrogel forms to load and deliver exosomes. Unlike decellularized matrix hydrogels, these scaffolds exhibit significantly slower degradation rates in vivo, ensuring a sustained release of adsorbed exosomes [42,43]. Moreover, decellularized matrix scaffolds do not require the introduction of additional synthetic components, which helps maintain low immunogenicity. Although there are currently no reports comparing the advantages and disadvantages of other decellularized matrix scaffolds (such as decellularized dermal matrix scaffolds) with decellularized pericardial scaffolds regarding exosome loading, several studies provide some insights: (1) Most studies currently employ co-incubation methods to anchor exosomes onto the collagen components of decellularized matrix scaffolds [44]. However, due to the considerable thickness of large decellularized matrix scaffolds, co-incubation may not ensure a uniform distribution of exosomes throughout the scaffold. In contrast, decellularized pericardial materials, which are thinner, allow exosomes to bind uniformly within their pores during co-incubation [43,45]. Consequently, after implantation, the exosomes carried by decellularized pericardial materials can be released slowly and uniformly, whereas thicker decellularized matrix scaffolds struggle to release exosomes evenly, which may reduce their bioavailability. (2) Decellularized matrix scaffolds loaded with exosomes serve two primary functions: first, exosomes recruit adipose-derived stem cells or epithelial progenitor cells, promoting their

proliferation and differentiation [46]; second, the decellularized matrix scaffold provides a venue for these cells to exert their biological functions. Recent studies have shown that decellularized matrix scaffolds of significant volume or thickness can create an ideal microenvironment for adipose-derived stem cells or epithelial progenitor cells, yet cell distribution tends to be concentrated at the edges of the large-volume scaffolds, with little evident recellularization in the core [42]. Another study found that thinner, membrane-like decellularized pericardial membranes achieve rapid recellularization on both their surface and interior after implantation, which offers another advantage of combining with exosomes: they can provide a more favorable scaffold (microenvironment) for cells involved in wound repair [47]. (3) The release of exosomes is primarily related to the degradation of their attachment structures, specifically the collagen in the scaffold. Due to the unique arrangement of collagen and elastin within decellularized pericardial membranes, they exhibit high resistance to degradation, which also provides strong mechanical properties [48]. Therefore, when an equivalent amount of exosomes is bound to either decellularized pericardial scaffolds or other decellularized matrix scaffolds, the exosomes released from the decellularized pericardial materials tend to be released more slowly and persistently over the same time period [27]. This characteristic can further enhance the bioavailability of exosomes.

In tissue repair and regenerative surgery, the insufficient availability of graft sources remains a significant clinical challenge. Decellularized materials eliminate biological factors such as cells that may lead to allogeneic tissue rejection while retaining proteins related to tissue regeneration, making them highly sought-after biomaterials in the field of tissue regeneration. The porcine pericardial decellularized matrix, commonly used in research, offers unique advantages as a wound dressing. In our study, the porcine pericardial decellularized matrix treated with a combination of Triton X-100 and pepsin digestion demonstrated effective decellularization, successfully removing the cellular structure from the pericardium. Other studies have shown that the structure, mechanical properties, and other characteristics of animal-derived xenograft decellularized pericardium closely resemble those of human pericardium [49]. Additionally, it fulfills all the characteristics of biomimetic materials and surpasses other materials in terms of mechanical strength, swelling behavior, and degradation properties [50]. Our experimental results indicate that the bilayer patches, which incorporate a collagen layer containing adipose stem cell exosomes, retained these beneficial properties, making them suitable for wound dressing applications. Cytocompatibility of biomaterials is another critical aspect; thus, decellularized matrices treated with chemical or biological agents must ensure the complete removal of residual reagents to guarantee their biocompatibility [51].

Currently, the effectiveness of other acellular matrix biomaterials in treating refractory wounds has been confirmed by numerous studies [52], several acellular matrix biomaterials products have already been marketed and applied in clinical practice, such as the acellular dermal matrix [53]. This is not only due to the fact that acellular dermal matrix is derived from natural tissue and has low immunogenicity, but also because it provides a favorable microenvironment for the biological functions of fibroblasts, keratinocytes, and vascular endothelial cells. However, recent studies have found that due to the inherent thickness of the dermal matrix, it is difficult to completely remove the internal cells and their contents, and residual substances (such as nucleic acids) may trigger a local immune response, leading to transplant failure [25]. In addition, although the thicker acellular dermal matrix can effectively cover the wound, its dense pores make it difficult to provide a convenient channel for wound exudate drainage and are not conducive to vascular ingrowth into the scaffold [54]. Moreover, the low collagen content of the acellular dermal matrix makes it more susceptible to degradation by enzymes in the body, reducing its tensile strength and increasing the risk of the wound rupture under significant mechanical stress.

Compared to acellular dermal matrix materials, acellular pericardial membrane materials have a higher collagen content (approximately 47 %) [48] and stronger tensile properties, with an elastic modulus closer to that of normal skin (1–5 MPa) [55]. In contrast to the degradation time of up to 4 weeks for acellular dermal matrix, the degradation rate of acellular pericardial membrane is significantly slower. Studies have shown that even 4–8 weeks after transplantation, the acellular pericardial membrane still retains considerable mechanical strength [47]. Additionally, the acellular pericardial membrane is thinner than the acellular dermal matrix and has larger pores, which facilitate wound exudate drainage and the formation of surrounding blood vessels [27]. More importantly, the loose and wide pores ensure thorough removal of cells and nucleic acids during the decellularization process, reducing the immunogenicity of the material [54]. Moreover, acellular pericardial membrane materials are also advantageous due to their low cost and easy availability [44].

In this study, the decellularized matrix we prepared not only demonstrated no cytotoxicity but also exhibited favorable properties that support cell proliferation, migration, and tube formation, thereby facilitating the growth of skin-associated cells (e.g., fibroblasts and keratinocytes) at the wound site. This, in turn, promoted the formation of granulation tissue and re-epithelialization. Additionally, the decellularization process increased the pore size of the tissue, and the cardiac-derived decellularized material retained natural pro-angiogenic factors, which enhance cell adhesion and angiogenesis. The natural structure of the extracellular matrix supports the exchange of important cellular signals during cell growth, further promoting blood vessel formation and tissue regeneration. We utilized porcine pericardial decellularized matrix combined with adipose stem cell exosomes for the first time to treat difficult-to-heal wounds. The loose structure of the decellularized matrix facilitated the distribution and release of exosomes. The combination of exosomes and decellularized matrix derived from porcine pericardium proved effective in treating difficult-to-heal wounds. This synergistic approach allowed for a relatively slow and sustained release of therapeutic agents compared to the use of exosomes alone.

Regarding why the decellularized pericardium can release exosomes relatively slowly and continuously exert therapeutic effects, we reviewed the literature and found that exosomes can anchor onto collagen in the extracellular matrix via cell adhesion molecules or integrin receptors [56–58]. Since the collagen content in decellularized pericardium (approximately 47 %) [48] is significantly higher than that in other decellularized matrix materials of the same mass, the decellularized pericardium has a greater drug-loading capacity for exosomes. Additionally, the decellularized pericardium is relatively loose with large pores, and studies have shown that such loose and wide pores can further increase its drug-loading capacity and facilitate the slow release of exosomes [27]. Moreover, the release of exosomes depends on enzymes in the body's microenvironment; only when collagenase continuously degrades the ECM can exosomes be gradually released. Therefore, the collagen content also determines the duration and rate of exosome release [59]. Research shows that commonly used wound healing materials, such as decellularized dermal matrix, degrade within 4 weeks in vivo [60], while the decellularized pericardium remains intact for 4–8 weeks, still exhibiting strong tensile strength, which demonstrates its excellent anti-degradation properties [47]. In conclusion, the large and loose pores, strong anti-degradation ability, and high collagen content of the pericardium contribute to its greater drug-loading capacity and longer release time, enabling the composite material to exert long-lasting therapeutic effects.

The decellularized matrix and exosomes exerted a simultaneous role in promoting wound healing. In this study, the pericardial decellularized matrix-collagen patches alone had significant effects in promoting cell proliferation migration, tubule formation, and collagen synthesis, and the exosome-loaded bilayer patches improved the rate and quality of wound healing by promoting granulation tissue formation, reepithelialization, angiogenesis, and collagen synthesis, which resulted in the convergence of mouse wounds to the normal non-diabetic healing

process. In recent years, in many studies of exosome-carrying biomaterials, the focus is not only on the carrying and release of exosomes, but also on the improvement of the materials to achieve better synergistic therapeutic purposes. The material used in this study not only releases exosomes, but also plays a role in promoting cell proliferation, migration and collagen synthesis. In our future research, we will focus on the fate of bilayer matrix patches and their material modification pathways, such as antimicrobial properties.

The innovation of this article is reflected in the following aspects: (1) Although the combination of exosomes and decellularized porcine pericardial matrix has been applied in myocardial regeneration [29], there is currently no research using the same biomaterials to treat diabetic refractory wounds.Our study preliminarily explores the effect of exosome-loaded bilayer patches on difficult-to-heal wounds, thereby expanding their application context. (2) As you mentioned, the concepts and research methods in this paper are similar to previous studies; however, we have clearly outlined the fundamental biological processes by which the patches promote wound healing, including granulation tissue regeneration, angiogenesis, epithelial cell migration, and collagen deposition. Additionally, we screened the dose of exosomes delivered by the decellularized porcine pericardial matrix to optimize these biological effects, which distinguishes our work from previous studies. (3) Investigating the potential mechanisms of biomaterials in treating refractory wounds not only enhances the readers' confidence in their therapeutic effects but also represents an innovation in the study. After clarifying the therapeutic effects of exosome-loaded bilayer patches on refractory wounds, we employed transcriptome sequencing technology to analyze the regenerated tissue, initially hypothesizing potential molecular mechanisms or signaling pathways that facilitate tissue repair. Further studies, including immunohistochemical staining, confirmed that the bilayer patches regulate macrophage polarization in the wound microenvironment, increasing the proportion of anti-inflammatory M2 macrophages and promoting tissue repair and regeneration. Additionally, molecular biology techniques clarified that the bilayer patches promote tissue re-epithelialization and collagen deposition by activating the cAMP signaling pathway, elucidating the molecular mechanisms and signaling pathways through which these patches treat refractory wounds.

Moreover, although our study has demonstrated the therapeutic effect of bilayer patches composed of collagen from adipose stem cell-derived exosomes and decellularized matrix from porcine pericardium on wounds in diabetic mice, the underlying mechanisms remain to be explored. Regarding the mechanism by which ADSC-exos promote angiogenesis, collagen deposition, and re-epithelialization in wound healing, studies have shown that ADSC-exos enhance the proliferation and migration of HUVECs, fibroblasts, and HaCaT cells by delivering the active component [61]. Additionally, they regulate the expression of VEGFA [62], HIF1α [63], and FGF4 in HUVECs through signaling molecules such as miR-204-3p [61], miR-146a-5p [62], miR-21 [16,38,64], circ-Astn1 [65], miR-144-3p [66], linc00511 [67], miR-106a-5p [68], and activate the p38 MAPK pathway, thereby enhancing the angiogenic capacity of HUVECs [32,63]. Moreover, ADSC-exos protect and enhance the functions of fibroblasts and HaCaT cells [69]. ADSC-exos also regulate the expression levels of HSP90, SIRT3, ANG1, FILK1, and VEGF proteins in cells, activate the AKT/ERK signaling pathway, inhibit the levels of reactive oxygen species (ROS) in a high-glucose environment, and reduce cell apoptosis [69,70]. Lastly, ADSC-exos can modulate the levels of IL-6, IL-1β, and TNF-α in the microenvironment, suppress inflammatory responses, and promote the polarization of macrophages toward the M2 phenotype [63]. In summary, ADSC-exos promote the healing of diabetic wounds by influencing biological processes such as angiogenesis, fibroblast and keratinocyte proliferation and migration, reducing apoptosis in these cells, and promoting M2 polarization of macrophages, as shown below figure [32].

In addition, regarding the mechanism by which decellularized pericardium materials promote angiogenesis, collagen deposition, and re-epithelialization in wound healing: (1) After the decellularized pericardium is transplanted into the wound, it recruits macrophages to infiltrate the wound area [71]. During the first 3 days, the infiltrating macrophages are predominantly pro-inflammatory M1 types. From days 3–7, the decellularized pericardium rapidly induces the polarization of M1 macrophages into anti-inflammatory M2 macrophages. The latter can secrete cytokines such as IL-10 and VEGF, promoting the proliferation and migration of keratinocytes and fibroblasts, thus accelerating early wound closure [54]. Fibroblasts further synthesize and secrete mature elastin and type I collagen, facilitating the formation of vascularized granulation tissue and providing the wound with tensile strength, helping prevent wound re-rupture [54]. (2) The decellularized pericardium promote keratinocytes and mucosal epithelial cells express β-defensin-1, S100A9, and antimicrobial peptides (AMPs), which directly or indirectly eliminate bacterial microorganisms and prevent the formation of bacterial biofilms [54]. Among these, β-defensin-1 is an atypical chemokine that mediates the activation of dendritic cells and T cells, thereby clearing microorganisms from the wound [72]. AMPs, secreted by keratinocytes, directly disrupt bacteria and viruses [72], while S100A9 is a calcium-binding protein with antibacterial properties, inhibiting the growth of various bacteria inside and outside cells and supporting leukocyte recruitment to the injury site to enhance the immune response [73]. (3) The decellularized pericardium has a loose and porous structure, which not only facilitates the drainage of wound exudate and nutrient exchange but also provides a favorable microenvironment for angiogenesis, fibroblast proliferation, and keratinocyte migration [27].

5. Conclusion

We have investigated a natural wound dressing that effectively delivers adipose-derived stem cell exosomes while gradually releasing them. Additionally, the decellularized matrix itself contributes to promoting wound healing. Based on this study, we anticipate that these dressing products can be clinically translated and applied to the treatment of chronic, hard-to-heal wounds. This approach aims to address the challenges of frequent dressing changes, poor clinical outcomes, and unfavorable prognoses associated with these conditions, providing a theoretical foundation for solving the issues related to the treatment of chronic hard-to-heal wounds.

CRediT authorship contribution statement

Wei Liang: Writing – review & editing, Writing – original draft, Investigation, Funding acquisition, Formal analysis, Data curation, Conceptualization. **Huiting Wu:** Writing – original draft, Software, Methodology, Formal analysis, Data curation. **Lindan Tan:** Methodology, Formal analysis. **Xiaoyu Meng:** Investigation, Data curation. **Wanwen Dang:** Investigation, Data curation. **Meng Han:** Investigation, Data curation. **Yonghuan Zhen:** Methodology, Investigation, Data curation. **Haifeng Chen:** Writing – review & editing, Conceptualization. **Hongsen Bi:** Data curation, Funding acquisition, Investigation. **Yang An:** Writing – review & editing, Funding acquisition, Conceptualization.

Declaration of competing interest

The authors have no financial interest to declare in relation to the content of this article.

Acknowledgement

This work was supported by Key Clinical Projects of Peking University Third Hospital (No. BYSYZD2021020), Postdoctoral Fellowship Program of CPSF (No. GZC20230151), the National Natural Science Foundation of China (No. 82070286), China Postdoctoral Science Foundation (2024M750129) and the Peking University Medicine Sailing

Program for Young Scholars' Scientific & Technological Innovation (No. BMU2024YFJHPY030).

Appendix A. Supplementary data

Supplementary data to this article can be found online at https://doi.org/10.1016/j.mtbio.2024.101398.

Data availability

Data will be made available on request.

References

[1] K. Las Heras, M. Igartua, E. Santos-Vizcaino, et al., Chronic wounds: current status, available strategies and emerging therapeutic solutions, J. Contr. Release 328 (2020) 532–550.

[2] K.D. Verma, F. Lewis, M. Mejia, et al., Food and Drug Administration perspective: Advancing product development for non-healing chronic wounds, Wound Repair Regen. 30 (2022) 299–302.

[3] J.D. Lehrman, Combining the benefits of collagen and negative pressure wound therapy to heal a chronic diabetic foot ulcer: a case report, Wounds 32 (2020) E11–e13.

[4] W. Qin, K. Liu, H. Su, et al., Tibial cortex transverse transport promotes ischemic diabetic foot ulcer healing via enhanced angiogenesis and inflammation modulation in a novel rat model, Eur. J. Med. Res. 29 (2024) 155.

[5] L. Macri, R.A. Clark, Tissue engineering for cutaneous wounds: selecting the proper time and space for growth factors, cells and the extracellular matrix, Skin Pharmacol. Physiol. 22 (2009) 83–93.

[6] A. Sadeghianmaryan, N. Ahmadian, S. Wheatley, et al., Advancements in 3D-printable polysaccharides, proteins, and synthetic polymers for wound dressing and skin scaffolding - a review, Int. J. Biol. Macromol. 266 (2024) 131207.

[7] G. Cossu, M. Birchall, T. Brown, et al., Lancet Commission: stem cells and regenerative medicine, Lancet 391 (2018) 883–910.

[8] H. Ma, W.S. Siu, P.C. Leung, The potential of MSC-based cell-free therapy in wound healing-A thorough literature review, Int. J. Mol. Sci. 24 (2023).

[9] X. Li, X. Xie, W. Lian, et al., Exosomes from adipose-derived stem cells overexpressing Nrf2 accelerate cutaneous wound healing by promoting vascularization in a diabetic foot ulcer rat model, Exp. Mol. Med. 50 (2018) 1–14.

[10] H. Yu, Y. Wu, B. Zhang, et al., Exosomes derived from E2F1(-/-) adipose-derived stem cells promote skin wound healing via miR-130b-5p/TGFBR3 Axis, Int. J. Nanomed. 18 (2023) 6275–6292.

[11] L. Qian, L. Pi, B.R. Fang, et al., Adipose mesenchymal stem cell-derived exosomes accelerate skin wound healing via the lncRNA H19/miR-19b/SOX9 axis, Lab. Invest. 101 (2021) 1254–1266.

[12] J. Zhu, H. Quan, Adipose-derived stem cells-derived exosomes facilitate cutaneous wound healing by delivering XIST and restoring discoidin domain receptor 2, Cytokine 158 (2022) 155981.

[13] Y. He, Q. Li, F. Feng, et al., Extracellular vesicles produced by human-induced pluripotent stem cell-derived endothelial cells can prevent arterial stenosis in mice via autophagy regulation, Front Cardiovasc Med 9 (2022) 922790.

[14] C. Long, J. Wang, W. Gan, et al., Therapeutic potential of exosomes from adipose-derived stem cells in chronic wound healing, Front Surg 9 (2022) 1030288.

[15] P.A. Shiekh, A. Singh, A. Kumar, Exosome laden oxygen releasing antioxidant and antibacterial cryogel wound dressing OxOBand alleviate diabetic and infectious wound healing, Biomaterials 249 (2020) 120020.

[16] Y. An, F. Huang, X. Tan, et al., Exosomes of adipose tissue-derived stem cells promote wound healing by sponging miR-17-5p and inducing autophagy protein Ulk1, Plast. Reconstr. Surg. 151 (2023) 1016–1028.

[17] K. Tjoa, M.H. Nadhif, S.S. Utami, et al., Mechanical, optical, chemical, and biological evaluations of fish scale-derived scaffold for corneal replacements: a systematic review, Int. J. Biol. Macromol. 267 (2024) 131183.

[18] M. Hu, S. Shi, X. Peng, et al., A synergistic strategy of dual-crosslinking and loading intelligent nanogels for enhancing anti-coagulation, pro-endothelialization and anti-calcification properties in bioprosthetic heart valves, Acta Biomater. 171 (2023) 466–481.

[19] K. Schenke-Layland, O. Vasilevski, F. Opitz, et al., Impact of decellularization of xenogeneic tissue on extracellular matrix integrity for tissue engineering of heart valves, J. Struct. Biol. 143 (2003) 201–208.

[20] S.B. Seif-Naraghi, M.A. Salvatore, P.J. Schup-Magoffin, et al., Design and characterization of an injectable pericardial matrix gel: a potentially autologous scaffold for cardiac tissue engineering, Tissue Eng Part A 16 (2010) 2017–2027.

[21] M. Monguió-Tortajada, C. Prat-Vidal, M. Moron-Font, et al., Local administration of porcine immunomodulatory, chemotactic and angiogenic extracellular vesicles using engineered cardiac scaffolds for myocardial infarction, Bioact. Mater. 6 (2021) 3314–3327.

[22] H.M. El-Husseiny, E.A. Mady, T. Usui, et al., Adipose stem cell-seeded decellularized porcine pericardium: a promising functional biomaterial to synergistically restore the cardiac functions post-myocardial infarction, Vet Sci 10 (2023).

[23] T. Yu, C. Zheng, X. Chen, et al., A universal strategy for the construction of polymer brush hybrid non-glutaraldehyde heart valves with robust anti-biological contamination performance and improved endothelialization potential, Acta Biomater. 160 (2023) 87–97.

[24] R.A. Grandis, L.N. Miotto, L.E. Genaro, et al., In vitro evaluation of acellular collagen matrices derived from porcine pericardium: influence of the sterilization method on its biological properties, Materials 14 (2021).

[25] S.F. Badylak, T.W. Gilbert, Immune response to biologic scaffold materials, Semin. Immunol. 20 (2008) 109–116.

[26] S. Yu, X. Chen, Y. Liu, et al., Exosomes derived from stem cells from the apical papilla alleviate inflammation in rat pulpitis by upregulating regulatory T cells, Int. Endod. J. 55 (2022) 517–530.

[27] M. Khazaei, M. Alizadeh, L. Rezakhani, Resveratrol-loaded decellularized ovine pericardium: ECM introduced for tissue engineering, Biotechnol. Appl. Biochem. 71 (2023) 387–401.

[28] L. Wang, J.A. Johnson, Q. Zhang, et al., Combining decellularized human adipose tissue extracellular matrix and adipose-derived stem cells for adipose tissue engineering, Acta Biomater. 9 (2013) 8921–8931.

[29] M. Monguió-Tortajada, C. Prat-Vidal, D. Martínez-Falguera, et al., Acellular cardiac scaffolds enriched with MSC-derived extracellular vesicles limit ventricular remodelling and exert local and systemic immunomodulation in a myocardial infarction porcine model, Theranostics 12 (2022) 4656–4670.

[30] W. Liang, M. Han, G. Li, et al., Perfusable adipose decellularized extracellular matrix biological scaffold co-recellularized with adipose-derived stem cells and L6 promotes functional skeletal muscle regeneration following volumetric muscle loss, Biomaterials 307 (2024) 122529.

[31] W. Zhang, X. Bai, B. Zhao, et al., Cell-free therapy based on adipose tissue stem cell-derived exosomes promotes wound healing via the PI3K/Akt signaling pathway, Exp. Cell Res. 370 (2018) 333–342.

[32] K. Wang, Z. Yang, B. Zhang, et al., Adipose-derived stem cell exosomes facilitate diabetic wound healing: mechanisms and potential applications, Int. J. Nanomed. 19 (2024) 6015–6033.

[33] S.F. Badylak, J.L. Dziki, B.M. Sicari, et al., Mechanisms by which acellular biologic scaffolds promote functional skeletal muscle restoration, Biomaterials 103 (2016) 128–136.

[34] J.G. Tidball, S.A. Villalta, Regulatory interactions between muscle and the immune system during muscle regeneration, Am. J. Physiol. Regul. Integr. Comp. Physiol. 298 (2010) R1173–R1187.

[35] Q. Du, A. Dickinson, P. Nakuleswaran, et al., Targeting macrophage polarization for reinstating homeostasis following tissue damage, Int. J. Mol. Sci. 25 (2024).

[36] T. Sang, Y. Wang, Z. Wang, et al., NEAT1 deficiency promotes corneal epithelial wound healing by activating cAMP signaling pathway, Investigative Opthalmology & Visual Science 65 (2024).

[37] Z. Wang, X. Wang, L. Fu, et al., Shengmai San formula alleviates high-fat diet-induced obesity in mice through gut microbiota-derived bile acid promotion of M2 macrophage polarization and thermogenesis, Phytomedicine 133 (2024) 155938.

[38] N. Liu, Y. Xie, Y. Zhen, et al., Free-cell therapeutics and mechanism of exosomes from adipose-derived stem cells in promoting wound healing: current understanding and future applications, Chin. Med. J. 135 (2022) 1803–1805.

[39] T. Frazier, A. Alarcon, X. Wu, et al., Clinical translational potential in skin wound regeneration for adipose-derived, blood-derived, and cellulose materials: cells, exosomes, and hydrogels, Biomolecules 10 (2020).

[40] Z. Wang, X. Liang, G. Wang, et al., Emerging bioprinting for wound healing, Adv. Mater. (2023) e2304738.

[41] Y. Cao, B. Chen, Q. Liu, et al., Dissolvable microneedle-based wound dressing transdermally and continuously delivers anti-inflammatory and pro-angiogenic exosomes for diabetic wound treatment, Bioact. Mater. 42 (2024) 32–51.

[42] S. Jiang, G. Tian, Z. Yang, et al., Enhancement of acellular cartilage matrix scaffold by Wharton's jelly mesenchymal stem cell-derived exosomes to promote osteochondral regeneration, Bioact. Mater. 6 (2021) 2711–2728.

[43] S. Xiao, C. Xiao, Y. Miao, et al., Human acellular amniotic membrane incorporating exosomes from adipose-derived mesenchymal stem cells promotes diabetic wound healing, Stem Cell Res. Ther. 12 (2021).

[44] D. Di Francesco, E. Marcello, S. Casarella, et al., Characterization of a decellularized pericardium extracellular matrix hydrogel for regenerative medicine: insights on animal-to-animal variability, Front. Bioeng. Biotechnol. 12 (2024).

[45] A.R. Khalatbary, M. Omraninava, D. Nasiry, et al., Exosomes derived from human adipose mesenchymal stem cells loaded bioengineered three-dimensional amniotic membrane-scaffold-accelerated diabetic wound healing, Arch. Dermatol. Res. 315 (2023) 2853–2870.

[46] C.H. Woo, H.K. Kim, G.Y. Jung, et al., Small extracellular vesicles from human adipose-derived stem cells attenuate cartilage degeneration, J. Extracell. Vesicles 9 (2020) 1735249.

[47] R. Khorramirouz, J.L. Go, C. Noble, et al., In vivo response of acellular porcine pericardial for tissue engineered transcatheter aortic valves, Sci. Rep. 9 (2019).

[48] R.A.D. Grandis, L.N. Miotto, L.E. Genaro, et al., In vitro evaluation of acellular collagen matrices derived from porcine pericardium: influence of the sterilization method on its biological properties, Materials 14 (2021).

[49] L. Iop, T. Palmosi, E. Dal Sasso, et al., Bioengineered tissue solutions for repair, correction and reconstruction in cardiovascular surgery, J. Thorac. Dis. 10 (2018) S2390–s2411.

[50] H. Wang, L. Ding, F. Xu, et al., Construction of novel amphiphilic chitosan-polylactide graft copolymer nanodroplets for contrast enhanced ultrasound tumor imaging, J. Biomater. Appl. 36 (2021) 613–625.

[51] J.A. Choe, S. Jana, B.J. Tefft, et al., Biomaterial characterization of off-the-shelf decellularized porcine pericardial tissue for use in prosthetic valvular applications, J Tissue Eng Regen Med 12 (2018) 1608–1620.

[52] C. Nie, G. Zhang, D. Yang, et al., Targeted delivery of adipose-derived stem cells via acellular dermal matrix enhances wound repair in diabetic rats, J Tissue Eng Regen Med 9 (2015) 224–235.
[53] L. Lingyan, Z. Han, L. Jialu, et al., Acellular dermal matrix for treatment of diabetic foot ulcer: an overview of systematic reviews, Int. J. Low. Extrem. Wounds (2023) 15347346231201696.
[54] M.S. El Masry, S. Chaffee, P. Das Ghatak, et al., Stabilized collagen matrix dressing improves wound macrophage function and epithelialization, Faseb. J. 33 (2018) 2144–2155.
[55] C.A. Grant, P.C. Twigg, D.J. Tobin, Static and dynamic nanomechanical properties of human skin tissue using atomic force microscopy: effect of scarring in the upper dermis, Acta Biomater. 8 (2012) 4123–4129.
[56] F. Stieglmeier, M. Grab, F. König, et al., Mapping of bovine pericardium to enable a standardized acquirement of material for medical implants, J. Mech. Behav. Biomed. Mater. 118 (2021) 104432.
[57] D. Di Francesco, C. Di Varsavia, S. Casarella, et al., Characterisation of matrix-bound nanovesicles (MBVs) isolated from decellularised bovine pericardium: new frontiers in regenerative medicine, Int. J. Mol. Sci. 25 (2024).
[58] Q. Xing, M. Parvizi, M. Lopera Higuita, et al., Basement membrane proteins modulate cell migration on bovine pericardium extracellular matrix scaffold, Sci. Rep. 11 (2021) 4607.
[59] C. Nataraj, G. Ritter, S. Dumas, et al., Extracellular wound matrices: novel stabilization and sterilization method for collagen-based biologic wound dressings, Wounds 19 (2007) 148–156.
[60] K.K. Mimura, A.R. Moraes, A.C. Miranda, et al., Mechanisms underlying heterologous skin scaffold-mediated tissue remodeling, Sci. Rep. 6 (2016) 35074.
[61] H. Huang, W. Zhu, Z. Huang, et al., Adipose-derived stem cell exosome NFIC improves diabetic foot ulcers by regulating miR-204-3p/HIPK2, J. Orthop. Surg. Res. 18 (2023) 687.
[62] D. Che, X. Xiang, J. Xie, et al., Exosomes derived from adipose stem cells enhance angiogenesis in diabetic wound via miR-146a-5p/JAZF1 Axis, Stem Cell Rev Rep 20 (2024) 1026–1039.
[63] R. Shi, Y. Jin, S. Zhao, et al., Hypoxic ADSC-derived exosomes enhance wound healing in diabetic mice via delivery of circ-Snhg11 and induction of M2-like macrophage polarization, Biomed. Pharmacother. 153 (2022) 113463.
[64] Y. An, J. Zhao, F. Nie, et al., Exosomes from adipose-derived stem cells (ADSCs) overexpressing miR-21 promote vascularization of endothelial cells, Sci. Rep. 9 (2019) 12861.
[65] Z. Wang, C. Feng, H. Liu, et al., Exosomes from circ-Astn1-modified adipose-derived mesenchymal stem cells enhance wound healing through miR-138-5p/SIRT1/FOXO1 axis regulation, World J. Stem Cell. 15 (2023) 476–489.
[66] N. Hu, Z. Cai, X. Jiang, et al., Hypoxia-pretreated ADSC-derived exosome-embedded hydrogels promote angiogenesis and accelerate diabetic wound healing, Acta Biomater. 157 (2023) 175–186.
[67] J. Qiu, C. Shu, X. Li, et al., Exosomes from linc00511-overexpressing ADSCs accelerates angiogenesis in diabetic foot ulcers healing by suppressing PAQR3-induced Twist1 degradation, Diabetes Res. Clin. Pract. 180 (2021) 109032.
[68] Z.H. Liang, N.F. Pan, S.S. Lin, et al., Exosomes from mmu_circ_0001052-modified adipose-derived stem cells promote angiogenesis of DFU via miR-106a-5p and FGF4/p38MAPK pathway, Stem Cell Res. Ther. 13 (2022) 336.
[69] S. Ren, J. Chen, J. Guo, et al., Exosomes from adipose stem cells promote diabetic wound healing through the eHSP90/LRP1/AKT Axis, Cells 11 (2022).
[70] Y. Zhang, X. Bai, K. Shen, et al., Exosomes derived from adipose mesenchymal stem cells promote diabetic chronic wound healing through SIRT3/SOD2, Cells 11 (2022).
[71] A. Das, S. Ghatak, M. Sinha, et al., Correction of MFG-E8 resolves inflammation and promotes cutaneous wound healing in diabetes, J. Immunol. 196 (2016) 5089–5100.
[72] M. Wolf, B. Moser, Antimicrobial activities of chemokines: not just a side-effect? Front. Immunol. 3 (2012) 213.
[73] S.Y. Lim, M.J. Raftery, C.L. Geczy, Oxidative modifications of DAMPs suppress inflammation: the case for S100A8 and S100A9, Antioxidants Redox Signal. 15 (2011) 2235–2248.